iScience

CellPress
OPEN ACCESS

Article

Bacteroides ovatus colonization influences the abundance of intestinal short chain fatty acids and neurotransmitters

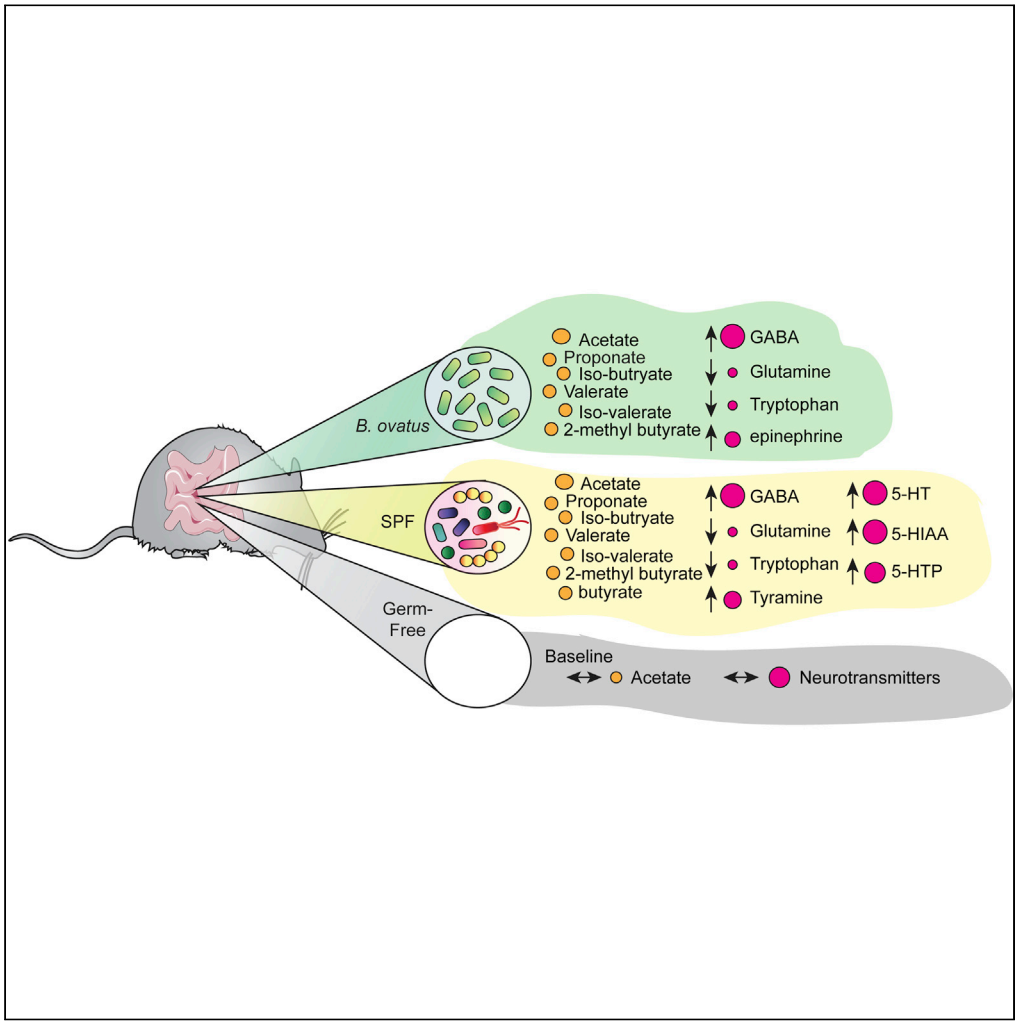

Thomas D. Horvath, Faith D. Ihekweazu, Sigmund J. Haidacher, ..., Anthony M. Haag, James Versalovic, Melinda A. Engevik

engevik@musc.edu

Highlights

Bacteroides ovatus modulates key neuro-active compounds *in vivo* in gnotobiotic animals

Horvath et al., iScience *25*, 104158
May 20, 2022
https://doi.org/10.1016/j.isci.2022.104158

iScience

CellPress
OPEN ACCESS

Article

Bacteroides ovatus colonization influences the abundance of intestinal short chain fatty acids and neurotransmitters

Thomas D. Horvath,[1,2,8] Faith D. Ihekweazu,[3,4,8] Sigmund J. Haidacher,[1,2] Wenly Ruan,[3,4] Kristen A. Engevik,[6] Robert Fultz,[5] Kathleen M. Hoch,[1,2] Ruth Ann Luna,[1,2] Numan Oezguen,[1,2] Jennifer K. Spinler,[1,2] Anthony M. Haag,[1,2] James Versalovic,[1,2] and Melinda A. Engevik[1,7,9,*]

SUMMARY

Gut microbes can synthesize multiple neuro-active metabolites. We profiled neuro-active compounds produced by the gut commensal *Bacteroides ovatus in vitro* and *in vivo* by LC-MS/MS. We found that *B. ovatus* generates acetic acid, propionic acid, isobutyric acid, and isovaleric acid. *In vitro*, *B. ovatus* consumed tryptophan and glutamate and synthesized the neuro-active compounds glutamine and GABA. Consistent with our LC-MS/MS-based *in vitro* data, we observed elevated levels of acetic acid, propionic acid, isobutyric acid, and isovaleric acid in the intestines of *B. ovatus* mono-associated mice compared with germ-free controls. *B. ovatus* mono-association also increased the concentrations of intestinal GABA and decreased the concentrations of tryptophan and glutamine compared with germ-free controls. Computational network analysis revealed unique links between SCFAs, neuro-active compounds, and colonization status. These results highlight connections between microbial colonization and intestinal neurotransmitter concentrations, suggesting that *B. ovatus* selectively influences the presence of intestinal neurotransmitters.

INTRODUCTION

The communication between gut microbiota and other organs has become an area of research that is rapidly developing. One key communication network is the gut-brain axis, which comprises the intestinal epithelium, the enteric nervous system (ENS), the autonomic nervous system, hypothalamic-pituitary-adrenal axis, and the central nervous system (CNS; Carabotti et al., 2015). This bidirectional communication is thought to regulate multiple aspects of human health. A leading concept of the gut-brain axis is that gut microbes secrete compounds that influence host signaling, affecting functions in both the gut and brain. The gut microbiota synthesizes a vast array of neuro-active metabolites that can communicate with the host. One well-characterized group of neuro-active metabolites are short chain fatty acids (SCFAs; Engevik and Versalovic, 2017), which include acetate, propionate, and butyrate. These SCFAs are reported to stimulate enteroendocrine cells, inhibit histone deacetylases, suppress inflammatory signals, and protect the blood-brain barrier from oxidative stress (De Vadder et al., 2014; Engevik et al., 2021; Gill et al., 2013; Hoyles et al., 2018; Nohr et al., 2013; Park et al., 2007, 2015, 2016, 2019a, 2019b; Stefanko et al., 2009; Vecsey et al., 2007).

Gut microbial metabolites appear to be crucial regulatory factors of the gut-brain axis. Specific microbial metabolites act as neuro-active molecules for the ENS and CNS. For example, select microbes secrete gamma-amino butyrate (GABA), tryptamine, dopamine, and norepinephrine (Cryan and Dinan, 2012; Galland, 2014; Pokusaeva et al., 2017; Williams et al., 2014). Studies have also shown that the gut microbiota can regulate the bioavailability of substrates required for the biosynthesis of host-derived neurotransmitters (Ma and Ma, 2019; Ney et al., 2017). Some intestinal microbes metabolize the essential amino acid tryptophan into kynurenine, quinolinate, indole, and indole derivatives, thereby limiting the availability of tryptophan for the host (Gao et al., 2018; Martin et al., 2018; O'Mahony et al., 2015). Microbial sequestration of tryptophan is suggested to reduce the bioavailability of tryptophan, limiting the host's production of neurotransmitters like serotonin (Gao et al., 2018; Waclawikova and El Aidy, 2018).

[1]Department of Pathology and Immunology, Baylor College of Medicine, Houston, TX, USA

[2]Department of Pathology, Texas Children's Hospital, Houston, TX, USA

[3]Department of Pediatrics, Baylor College of Medicine, Houston, TX, USA

[4]Section of Gastroenterology, Hepatology, and Nutrition, Texas Children's Hospital, Houston, TX, USA

[5]Department of Neuroscience, Cell Biology, and Anatomy, University of Texas Medical Branch, Galveston, TX, USA

[6]Department of Molecular Virology and Microbiology, Baylor College of Medicine, Houston, TX, USA

[7]Department of Regenerative Medicine & Cell Biology, Medical University of South Carolina, 173 Ashley Ave, BSB 621, Charleston, SC 29425, USA

[8]These authors contributed equally

[9]Lead contact

*Correspondence: engevik@musc.edu

https://doi.org/10.1016/j.isci.2022.104158

Bacteroides spp. are dominant members of the human gut microbiota (Eckburg et al., 2005; Engevik and Versalovic, 2017; Ley et al., 2005, 2006; Nguyen et al., 2015) with the genetic capacity to influence the gut-brain axis. They harbor an extensive repertoire of enzymes for carbohydrate fermentation, which generates volatile fatty acids and other metabolites (Wexler, 2007). *Bacteroides fragilis*, *Bacteroides caccae*, *Bacteroides vulgatus*, and *B. ovatus* produce the neurotransmitter GABA (Strandwitz et al., 2019), but the complete profile of *Bacteroides*-produced neuro-active compounds has yet to be elucidated. In fact, few studies have addressed the production of *Bacteroides*-derived neuro-active metabolites *in vivo*. In this study, we aimed to identify neuro-active metabolites produced by *B. ovatus* ATCC 8483, a human gut commensal bacterium with anti-inflammatory properties and next-generation probiotic potential (Ihekweazu et al., 2019, 2021; Tan et al., 2018). Given the prominent role of the microbiota in host health, deciphering the mechanisms of microbe-host crosstalk and how they impact health is of great importance and will improve our current understanding of the microbiome-gut-brain axis.

RESULTS

Genome analysis of *Bacteroides* spp. reveal the capacity to produce multiple neuro-active compounds

Commensal *Bacteroides* species are well-documented members of the human gut microbiota, but the precise roles these microbes play in modulating intestinal neurotransmitters and neuro-active compounds remain unclear. To examine the capacity of *Bacteroides* species to generate neuro-active metabolites, we surveyed enzymes related to neuro-active pathways in the genomes of 51 *Bacteroides* species using the Integrated Microbial Genomes (IMG) database (http://img.jgi.doe.gov) (see *Bacteroides* genomes in Table 1). We found that 32 of the 51 *Bacteroides* contained EC 4.1.1.15 (glutamate decarboxylase) that is required to produce GABA from glutamate (Figures 1A and 1B). GABA can also be generated from succinate and we identified four *Bacteroides* species harboring EC 1.2.1.16 (succinate-semialdehyde dehydrogenase) and three species harboring EC 2.6.1.19 (GABA transaminase); suggesting that some *Bacteroides* species can synthesis GABA from succinate.

We identified that all of the *Bacteroides* contained EC 6.3.1.2 (glutamine synthetase) that converts glutamate and ammonia into glutamine, and EC 1.4.1.13 (glutamate synthase) that converts glutamine into glutamate (Figures 1A and 1B). We found that the majority of *Bacteroides* species had the ECs involved in sequentially converting chorismate to tyrosine EC 5.4.99.5, chorismate mutase (51 genomes), EC 1.3.1.12, prephenate dehydrogenase (46 genomes), and EC 2.6.1.1, aspartate transaminase (51 genomes). Lastly, 49 of the 51 *Bacteroides* species had EC 4.1.1.11 (aspartate 1-decarboxylase), which is required for tyramine production. Importantly, we identified that all 22 of the *B. ovatus* genomes had the ECs for generating GABA, glutamate, glutamine, indole, and tyrosine (Figures 1A and 1B). Two of the *B. ovatus* genomes were also able to generate GABA from succinate (EC 1.2.1.16).

In terms of SCFA production, the majority of *Bacteroides* species harbored the ECs for acetate production, including EC 1.2.7.1 (pyruvate synthase, 51 genomes), EC 2.7.2.1 (acetate kinase, 51 genomes), EC 1.2.7.11 (2-oxoacid oxidoreductase, 49 genomes), and EC 6.2.1.1 (acetyl-CoA synthetase, 45 genomes) (Figure 1C). Enzymes required for propionate, EC 2.7.2.1 (acetate kinase, 51 genomes) and butyrate production, EC 2.7.2.7 (butyrate kinase, 48 genomes), were also identified in *Bacteroides*. Of note, all *B. ovatus* genomes could produce acetate, propionate, and butyrate (Figure 1C). These data suggest that many, but not all, *Bacteroides* species harbor the enzymatic machinery to produce several neuro-active compounds including GABA, glutamate, glutamine, tyrosine, tyramine, and SCFAs.

Bacteroides ovatus generates several SCFAs and neuro-active compounds *in vitro*

Based on the results of our *Bacteroides* genome surveillance we used LC-MS/MS to test whether *B. ovatus* ATCC 8483 could synthesize SCFAs and the neuro-active compounds GABA, glutamine, and tyrosine *in vitro* (Tables 2, 3, 4, and 5). We cultured *B. ovatus* ATCC 8483 in ZMB1, a fully defined medium that mirrors the gut in terms of amino acid and carbohydrate availability (Figure 2A). The ZMB1 at baseline contains 0.16 mM acetic acids and 0 mM of all other SCFAs. Our data showed that *B. ovatus* ATCC 8483 secreted high concentrations of acetic acid (acetate: 1.3 $\pm$ 0.2 mM) above the ZMB1 baseline and propionic acid (propionate: 0.7 $\pm$ 0.1 mM), and, to a much lower degree, iso-butyric acid (iso-butyrate: 24.3 $\pm$ 2.2 μM), isovaleric acid (iso-valerate: 15.5 $\pm$ 1.3 μM), butyric acid (butyrate: 4.6 $\pm$ 2.2 μM), and 2-methyl butyric acid (2.1 $\pm$ 0.4 μM) (Figure 2B). Analysis of neurotransmitter concentrations revealed that *B. ovatus* secreted high concentrations of GABA (281.7 $\pm$ 4.9 μg/mL) (Figure 2C), and moderate concentrations of

Table 1. *Bacteroides* genomes identified from the JGI Integrated Microbial Genomes (IMG) database (http://img.jgi.doe.gov)

Bacteroides	JGI Genome #
B. acidifaciens	3
B. barnesiae	2
B. caccae	6
B. caecimuris	2
B. cellulosilyticus	6
B. clarus	4
B. coagulans	1
B. congonensis	1
B. coprophilus	4
B. coprosuis	1
B. cutis	1
B. dorei	5
B. eggerthii	4
B. faecichinchillae	2
B. faecis	2
B. finegoldii	5
B. fluxus	1
B. fragilis	107
B. galacturonicus	1
B. gallinarum	2
B. graminisolvens	2
B. helcogenes	1
B. heparinolyticus	2
B. ihuae	1
B. intestinalis	4
B. luti	1
B. massiliensis	3
B. mediterraneensis	1
B. neonati	1
B. nordii	2
B. oleiciplenus	1
B. ovatus	22
B. paurosaccharolyticus	1
B. pectinophilus	1
B. plebeius	1
B. propionicifaciens	2
B. pyogenes	6
B. reticulotermitis	2
B. rodentium	1
B. salyersiae	5
B. sartorii	3
Unclassified Bacteroides sp.	43
B. stercorirosoris	3
B. stercoris	8

(*Continued on next page*)

Table 1. *Continued*

Bacteroides	JGI Genome #
B. tectus	1
B. thetaiotaomicron	16
B. timonensis	1
B. uniformis	13
B. vulgatus	8
B. xylanisolvens	21
B. xylanolyticus	1
B. zoogleoformans	2

the neuro-active amino acid glutamine (85.3 ± 9.1 ng/mL). Interestingly, our data show that *B. ovatus* ATCC 8483 consumed the glutamate (−483.1 ± 6.83 μg/mL) present in the ZMB1 medium (original concentration: 787.0 μg/mL) (Figure 2C), which we speculate was used to drive GABA production. Analysis of metabolites in the tryptophan pathway revealed that *B. ovatus* also consumed the tryptophan (−54.8 ± 17.5 μg/mL) present in the ZMB1 medium (original concentration: 221.8 μg/mL). *B. ovatus* ATCC 8483 did not produce host-related 5-hydroxytryptamine (5-HT, serotonin), 5-hydroxyindoleacetic acid (5-HIAA), 5-hydroxytryptophan (5-HTP), or N-acetyl-5-methoxy tryptamine (melatonin) (Figure 2D). We also examined metabolites related to the tyramine/tyrosine/dopamine pathway and found that *B. ovatus* generated tyramine (120.7 ± 15.2 ng/mL) and tyrosine (11.7 ± 1.6 μg/mL), but not dopamine, norepinephrine, epinephrine, or anthranilic acid (Figure 2E). These data align with our genomic findings and suggest that *B. ovatus* is capable of producing several neuro-active compounds *in vitro*.

B. ovatus modulates SCFAs and neuro-active profiles *in vivo*

To address whether *B. ovatus* could synthesize the same SCFAs and neurotransmitter compounds *in vivo*, we mono-associated germ-free mice with *B. ovatus* ATCC 8483 to create gnotobiotic animals. As controls, we included germ-free mice (no gut microbiota) and specific pathogen free (SPF) mice with a conventional gut microbiota in our analysis (Figure 3A). Sequencing of 16S rRNA genes from gut contents of these animals confirmed that germ-free mice had no microbial community and that *B. ovatus* mono-associated mice only harbored *Bacteroides*. SPF mice were colonized with a complex microbial community dominated by *Lactobacillus* (45.4%), *Clostridium* XlVa (12.3%), *Flavonifractor* (5.5%), *Anaeroplasma* (4.7%) and *Parabacteroides* (4.6%), and other microbes (Figure 3B). Of note, *Bacteroides* made up only 2.2% of the conventional mouse gut microbiota. A closer examination of *Bacteroides* OTUs from SPF mice revealed that this group was dominated by *Bacteroides xylanisolvens* (OTU_45). Although we did not identify *B. ovatus* OTUs in our SPF mice by 16S sequencing, we would predict that *B. xylanisolvens* would have many of the same functions as *B. ovatus*, since this species contained the same ECs as *B. ovatus* in our genome analysis. We examined fecal SCFAs by LC-MS/MS to identify which SCFAs were generated in the presence of *B. ovatus* ATCC 8483 and a complex gut microbiota (Figure 3C). Consistent with previous literature, germ-free mice had low concentrations of acetic acid and no detectable levels of propionic acid, butyric acid, iso-butyric acid, valeric acid, iso-valeric acid, or 2-methyl butyric acid (Engevik et al., 2021). In contrast, *B. ovatus* mono-associated and SPF mice exhibited high concentrations of acetic acid and propionic acid, and lower amounts of iso-butyric acid, iso-valeric acid, and 2-methyl-butyric acid (Figure 3C). These findings mirror our *in vitro* findings (Figure 2B). Only SPF mice had detectable levels of butyric and valeric acid. Our data indicate that *B. ovatus* only produces some of the metabolites under investigation, whereas a more diverse microbiota produces additional compounds like butyrate.

Finally, we used our LC-MS/MS methods to examine key neuro-active metabolites and pathways from the feces of germ-free, *B. ovatus* mono-associated, and SPF mice. Similar to our *in vitro* findings, we observed that *B. ovatus* significantly increased colonic GABA (10.1 ± 7.9 ng/mg feces) compared with germ-free control mice (0.8 ± 0.3 ng/mg feces) (Figure 3D). Although we observed consumption of glutamate *in vitro*, *in vivo* we found that *B. ovatus* colonization had no effect on glutamate levels and decreased glutamine (27.9 ± 6.1 ng/mg feces) compared with germ-free controls (543.0 ± 59.2 ng/mg feces). SPF mice exhibited comparable levels of GABA and glutamine compared with *B. ovatus* mono-associated mice, suggesting that microbes within this complex community are capable of similar functions. Consistent with our *in vitro* findings, we also observed decreased levels of tryptophan in *B. ovatus* mono-associated mice

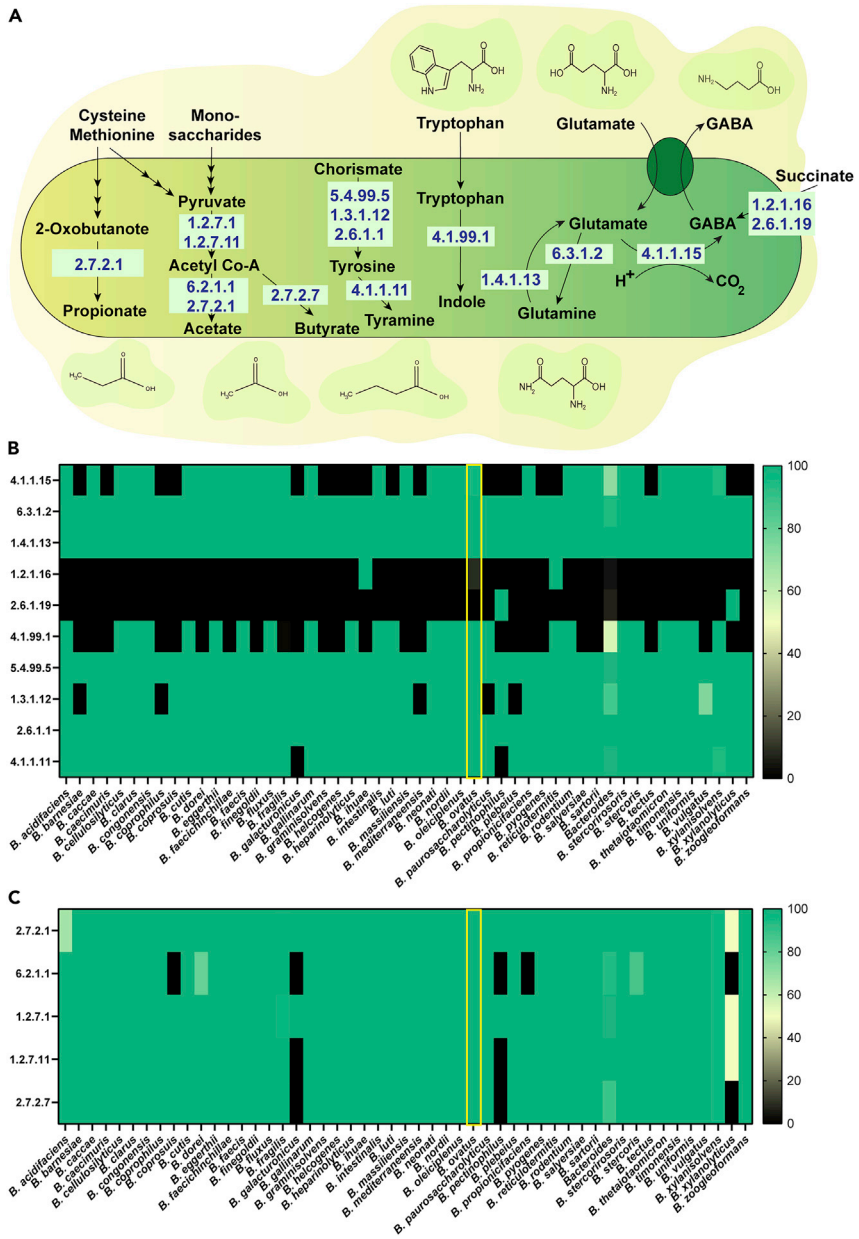

Figure 1. Genome analysis of the pathways involved in the production of neuroactive compounds in *Bacteroides* spp

(A) Gene pathways in *Bacteroides* were identified via the KEGG database (https://www.genome.jp/kegg/kegg2.html). Diagram of the pathways indicating enzyme commission (EC) numbers.

(B) Heat maps of the ECs involved in neuro-active compound production, as identified in the JGI Integrated Microbial Genomes (IMG) database (http://img.jgi.doe.gov). 51 Bacteroides species were identified, and the heat maps depict the percent (%) of strains that possessed the specific EC within each *Bacteroides* species. *B. ovatus* is highlighted with a yellow box.

(C) Heat maps of the ECs involved in short chain fatty acid (SCFA) production in each *Bacteroides* species as identified in the IMG database. *B. ovatus* is highlighted with a yellow box.

(10.9 ± 3.9 ng/mg feces) and SPF mice (12.0 ± 3.9 ng/mg feces) compared with germ-free controls (52.3 ± 12.5 ng/mg feces) (Figure 3E). *B. ovatus* did not affect host concentrations of serotonin, 5-HIAA, 5-HTP, melatonin, or tryptamine. In contrast, SPF mice exhibited significantly elevated serotonin, 5-HIAA, and 5-HTP compared with germ-free controls. Despite our *in vitro* findings, which indicated that *B. ovatus* could

Table 2. SRM transition parameters for the glutamate cycle metabolites on the Sciex 6500 QTrap MS

Metabolite	Q1 (*m/z*)	Q3 (*m/z*)[a]	DP (V)[b]	EP (V)[c]	CE (eV)[d]	CXP (V)[e]
GABA	104.1	87.1/69.1	80	9	20/30	9
d_6-GABA (IS)	110.1	92.1/73.1	80	9	20/30	9
glutamate	148.1	84.0/130.1	55	9	24/14	11
d_5-glutamate (IS)	153.1	88.1/135.1	55	9	24/14	11
glutamine	147.1	130.1/84.1	55	9	14/24	11
d_5-glutamine (IS)	152.1	135.1/88.1	55	9	14/24	11

[a]Corresponds to the mass-to-charge (*m/z*) of the quantifying fragment ion, and the red text corresponds to the *m/z* of the qualifying fragment ion.
[b]DP, declustering potential.
[c]EP, entrance potential.
[d]CE, collision energy.
[e]CXP, collision-cell exit potential; V, volts; eV, electron volts.

synthesize tyramine and tyrosine, our *in vivo* data revealed no differences in the tyramine or tyrosine concentrations between *B. ovatus* mono-associated mice and germ-free controls (Figure 3F). Interestingly, only *B. ovatus* mice had elevated epinephrine concentrations and only SPF mice harbored elevated concentrations of tyramine.

Network analysis reveals unique connections between *B. ovatus* colonization and neurotransmitter levels

Network analysis showed distinct connections between germ-free, *B. ovatus* mono-associated, and SPF mice in relation to SCFAs and neurotransmitter production (Figure 4A). Metabolite networking revealed

Table 3. SRM transition parameters for the N-phenyl SCFA derivatives on the Sciex 6500 QTrap MS

Metabolite	Q1 (*m/z*)	Q3 (*m/z*)[a]	DP (V)[b]	EP (V)[c]	CE (eV)[d]	CXP (V)[e]
N-phenyl acetamide	136.1	94.0/77.0	60	9	22/40	15
[$^{13}C_6$]-N-phenyl acetamide (IS)	142.1	100.0/84.0	60	10	22/51	15
N-phenyl propanamide	150.1	94.0/77.0	70	9	22/42	15
[$^{13}C_6$]-N-phenyl propanamide (IS)	156.1	100.0/82.9	60	10	26/45	15
N-phenyl butanamide[f]	164.1	94.0/77.0	75	9	23/45	15
[$^{13}C_6$]-N-phenyl butanamide (IS)	170.1	100.0/82.9	60	10	25/49	15
N-phenyl isobutanamide[f]	164.1	94.0/77.0	72	9	24/46	15
[$^{13}C_6$]-N-phenyl isobutanamide (IS)	170.1	100.0/82.9	72	9	24/46	15
N-phenyl 2-methylbutanamide[g]	178.1	94.0/77.0	80	9	23/49	15
[$^{13}C_6$]-N-phenyl 2-methylbutanamide (IS)	184.1	100.0/82.9	80	9	23/49	15
N-phenyl pentanamide[g]	178.1	94.0/77.0	80	9	23/48	15
[$^{13}C_6$]-N-phenyl pentanamide (IS)	184.1	100.0/82.9	80	9	23/48	15
N-phenyl isopentanamide[g]	178.1	94.0/77.0	80	9	23/49	15
[$^{13}C_6$]-N-phenyl isopentanamide (IS)	184.1	100.0/82.9	80	9	23/49	15

[a]Corresponds to the mass-to-charge (*m/z*) of the quantifying fragment ion, and the red text corresponds to the *m/z* of the qualifying fragment ion.
[b]DP, declustering potential.
[c]EP, entrance potential.
[d]CE, collision energy.
[e]CXP, collision-cell exit potential; V, volts; eV, electron volts.
[f]N-phenyl butanamide and N-phenyl isobutanamide, and their respective IS materials, are isobaric compounds and are resolved chromatographically.
[g]N-phenyl 2-methylbutanamide, N-phenyl pentanamide, and N-phenyl isopentanamide, and their respective IS materials, are all isobaric compounds and resolved chromatographically.

Table 4. SRM transition parameters for the Tryptophan Pathway metabolites on the Sciex 6500 QTrap MS

Metabolite	Q1 (*m/z*)	Q3 (*m/z*)[a]	DP (V)[b]	EP (V)[c]	CE (eV)[d]	CXP (V)[e]
tryptophan	205.1	188.1/146.1	35	7	15/25	15
d_5-tryptophan (IS)	210.1	192.1/150.1	35	7	15/25	15
serotonin	177.1	160.1/115.1	20	8	17/38	10
d_4-serotonin (IS)	181.1	164.1/119.1	20	8	17/38	10
melatonin	233.1	174.1/159.1	45	6	22/39	15
d_4-melatonin (IS)	237.1	178.1/163.1	45	6	22/39	15
5-hydroxy-indoleacetic acid (5-HIAA)	192.1	146.1/118.1	70	8	23/40	17
d_5-5-HIAA (IS)	197.1	150.1/122.1	70	8	23/40	17
5-hydroxy-tryptophan	221.1	204.1/162.1	40	7	16/26	23
N-acetylserotonin	219.1	160.1/115.1	40	8	23/49	10

[a]Corresponds to the mass-to-charge (*m/z*) of the quantifying fragment ion, and the red text corresponds to the *m/z* of the qualifying fragment ion.
[b]DP, declustering potential.
[c]EP, entrance potential.
[d]CE, collision energy.
[e]CXP, collision-cell exit potential; V, volts; eV, electron volts.

that *B. ovatus* colonization was uniquely associated with epinephrine, whereas SPF and *B. ovatus* colonization were both linked to GABA and acetic acid (Figure 4A). Moreover, SPF and *B. ovatus* colonization was linked to acetic acid, propionic acid, isobutyric acid, and 2-methyl-butryic acid. Interestingly, SPF mice alone had connections with butyric acid. GF mice had stronger associations with tyrosine, tryptophan, and glutamine than SPF and *B. ovatus* colonized mice. These correlations can also be visualized in the heatmap (Figure 4B), which highlights the differences between the groups. Collectively, these data indicate that *B. ovatus* modulates the presence of select neuro-active compounds and may participate in essential host communication networks.

DISCUSSION

Recent studies have established that members of the gut microbiota communicate with the intestinal epithelium, ENS, and CNS (Bercik et al., 2011, 2012; Carabotti et al., 2015; Clarke et al., 2013; Cryan and

Table 5. SRM transition parameters for the Tyrosine Pathway metabolites on the Sciex 6500 QTrap MS

Metabolite	Q1 (*m/z*)	Q3 (*m/z*)[a]	DP (V)[b]	EP (V)[c]	CE (eV)[d]	CXP (V)[e]
tyrosine	182.1	165.1/136.1	50	8	14/19	10
tyramine	138.1	121.1/103.1	40	8	16/29	10
d_4-tyramine (IS)	142.1	125.1/106.1	40	8	16/29	10
dopamine	154.1	137.1/91.1	40	9	15/32	10
d_4-dopamine (IS)	158.1	141.1/95.1	40	9	15/32	10
L-DOPA	198.1	181.1/152.1	50	7	14/20	9
d_3-L-DOPA (IS)	201.1	184.1/155.1	50	7	14/20	9
norepinephrine	170.1	152.1/107.1	40	9	26-Dec	9
epinephrine	184.1	166.1/151.1	40	8	15/30	15
d_6-epinephrine (IS)	190.1	172.1/157.1	40	8	15/30	15
anthranilic acid	138	120.0/92.0	30	4	16/38	12

[a]Corresponds to the mass-to-charge (*m/z*) of the quantifying fragment ion, and the red text corresponds to the *m/z* of the qualifying fragment ion.
[b]DP, declustering potential.
[c]EP, entrance potential.
[d]CE, collision energy.
[e]CXP, collision-cell exit potential; V, volts; eV, electron volts.

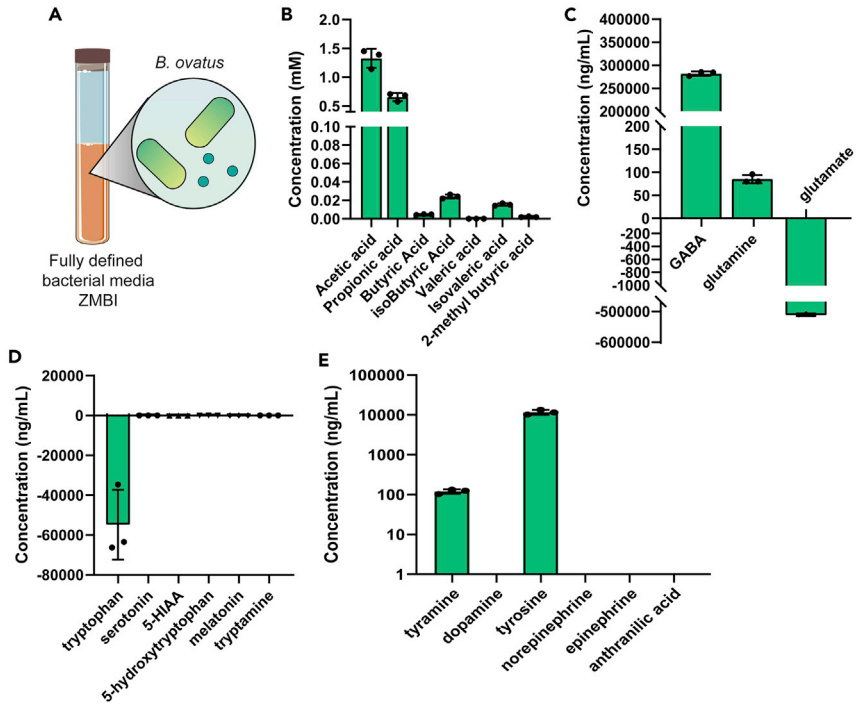

Figure 2. *B. ovatus* ATCC 8483 generates multiple neuroactive compounds *in vitro*

(A and B) Representative diagram of *B. ovatus* grown in the fully defined bacterial media ZMB1. (B) Concentrations of the SCFAs produced by *B. ovatus* in ZMB1 after overnight growth.

(C) Concentrations of metabolites produced by *B. ovatus* in ZMB1 in the Glutamate Cycle Pathway by LC-MS/MS.

(D) Concentrations of metabolites produced by *B. ovatus* in ZMB1 in the Tryptophan Pathway by LC-MS/MS.

(E) Concentrations of metabolites produced by *B. ovatus* in ZMB1 in the Tyrosine/dopamine Pathway by LC-MS/MS. All concentrations are shown after subtraction of baseline ZMB1 levels. For all experiments, $n = 3$ replicates; data are represented as mean +/− stdev.

Dinan, 2012; Engevik et al., 2021; Luck et al., 2020; Luk et al., 2018). However, at present, it is unclear how specific gut microbes communicate with the host. Microbial produced neuro-active compounds, many of which are neurotransmitters, can stimulate enteroendocrine cells and enteric neurons to activate important pathways. Whereas many studies have used complex microbial communities in SPF mice to dissect the role of the microbiota in modulating the host, these studies make it challenging to decipher which microbes are contributing to the host communication. In this study, we employed *B. ovatus* mono-associated gnotobiotic animals, which allowed us to directly assess which metabolites *B. ovatus* produces *in vivo*. To the best of our knowledge, this is the first work to systemically characterize neurotransmitter production *in vitro* and *in vivo* by *B. ovatus*. Our data indicate that *B. ovatus* synthesizes several SCFAs, secretes GABA, and modulates the levels of tryptophan and glutamine. Our data also indicate that *B. ovatus* does not affect the serotonin or dopamine pathways. These findings point to other gut microbes in the regulation of these systems. This work provides a more comprehensive view of how *Bacteroides* species may impact the gut and other organ systems.

Our data suggest that GABA production is a feature of *B. ovatus* colonization. In the gut, amino acid decarboxylation systems, such as the glutamate decarboxylase (GAD), enable bacterial species to cope with acid stress (Cotter et al., 2001; Sanders et al., 1998; Small and Waterman, 1998; Su et al., 2011). Glutamate decarboxylation via the bacterial GAD system results in production of GABA (Feehily and Karatzas, 2013; Pokusaeva et al., 2017; Sze, 1979). Similar to our findings, Matsumoto et al. found decreased levels of GABA in the stool and blood of germ-free mice compared with conventional (SPF) mice (Matsumoto et al., 2017). Fecal GABA levels are also decreased by antibiotic use (Fujisaka et al., 2018), suggesting that the microbiota is the main contributor to intestinal GABA. Analysis of the transcriptomics of human stool suggests that *Bacteroides* and *Parabacteroides* are the major contributors of intestinal GABA (Strandwitz et al., 2019). These human studies appear to be mirrored by *in vitro* work. For example, *B. ovatus* and *B. caccae* have been documented to produce GABA at

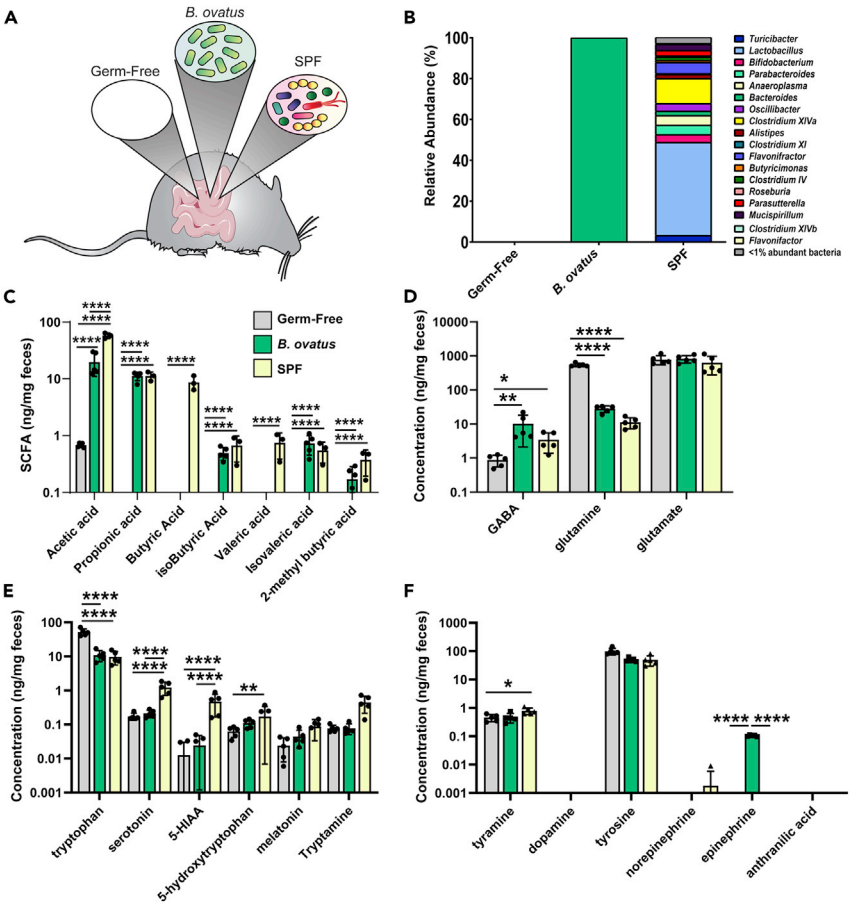

Figure 3. *B. ovatus* ATCC 8483 selectively modulates neuroactive compounds *in vivo*

(A and B) Representative diagram of animal experiments, depicting germ-free mice treated with PBS (germ-free), germ-free treated with *B. ovatus* (*B. ovatus* mono-associated), or specific pathogen free (SPF) mice that harbor a complete gut microbiota. B. 16S rRNA sequencing of germ-free, *B. ovatus* mono-associated, and SPF mice feces.

(C) Analysis of SCFAs measured from a known mass of stool (ng/mg wet stool weight) reflecting *in vivo* levels of SCFAs from germ-free, *B. ovatus* mono-associated mice, and SPF mice.

(D) Concentrations of metabolites in feces in the Glutamate/GABA/Glutamine Cycle Pathway by LC-MS/MS from a known mass of stool (ng/mg wet stool weight).

(E) Concentrations of metabolites in the Tryptophan Pathway by LC-MS/MS from a known mass of stool (ng/mg wet stool weight).

(F) Concentrations of metabolites in the tyrosine/dopamine/tyramine Pathway by LC-MS/MS from a known mass of stool (ng/mg wet stool weight). For all experiments, $n = 5$ mice/group for germ-free and *B. ovatus* colonized, $n = 5$ mice/group of SPF; data are represented as mean +/− stdev. Two-way ANOVA, $*p < 0.05$, $**p < 0.01$, $***p < 0.001$, $****p < 0.0001$.

pH six to seven, which represents the pH of the intestine (Strandwitz et al., 2019). This is consistent with our work in ZMB1 (pH = 6.5) and our gnotobiotic data. In the host, GABA is a primary inhibitory neurotransmitter (Hyland and Cryan, 2010; Wong et al., 2003) and has diverse physiologic effects, such as modulation of blood pressure (Chen and Bonham, 2010), immune function (Jin et al., 2013), excitability of colonic sensory afferents (Pokusaeva et al., 2017), and depression (Strandwitz et al., 2019). These health-modulating properties of GABA have fueled a growing interest in GABA-enriched dietary supplements and naturally fermented food products (Barrett et al., 2012). Our data suggest that *B. ovatus* can increase GABA levels *in vivo* and may provide a targeted microbial-based therapeutic for bolstering intestinal GABA levels. Future studies using mutants of *B. ovatus* that cannot generate GABA would be incredibly useful in dissecting the exact role of microbial GABA in modulating gut homeostasis.

Our data indicate that *B. ovatus* alone can elevate multiple neuroactive compounds *in vivo*. However, a complete gut microbiota with only 2% *Bacteroides* was able to produce similar or higher levels of all identified metabolites.

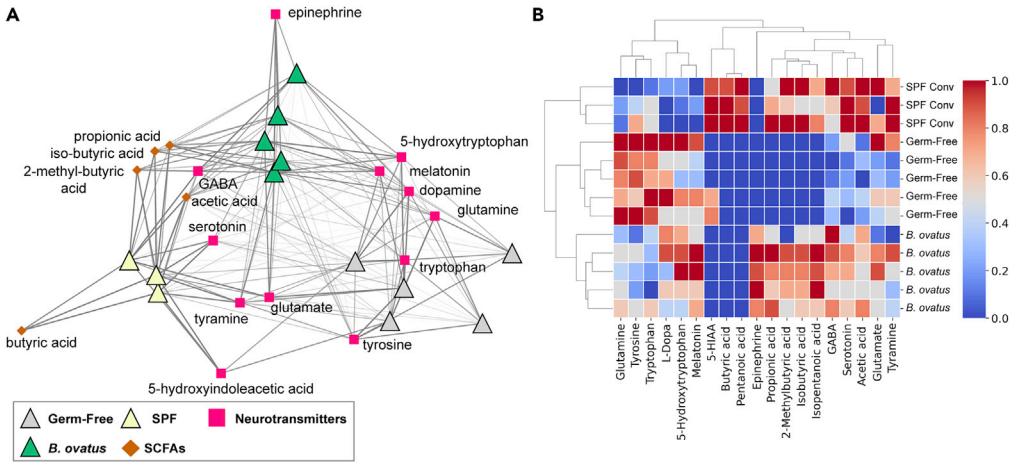

Figure 4. Network analysis reveals unique connections between germ-free, SPF, and *B. ovatus* colonized mice and key neuro-modulatory compounds

(A) Network analysis depicting neurotransmitters and short chain fatty acids (SCFA) profiles in germ-free (gray), *B. ovatus* mono-associated (green), or specific pathogen free (SPF; yellow) mice. Neurotransmitters are designated by pink squares and SCFAs by orange diamonds. The thickness of the lines is proportional to the concentration of the metabolites.

(B) Heatmap representation of the network analysis for SPF conventionalized mice, germ-free mice, and *B. ovatus* mono-associated mice.

We speculate that other species may be contributing to the same pool of neurotransmitters. For example, *Bifidobacteria* and to a lesser degree *Lactobacilli*, *Enterococci*, and *Streptococci* are also known to produce GABA (Cui et al., 2020; Pokusaeva et al., 2017). Acetate production is widely distributed among gut microbes (Morrison and Preston, 2016), whereas propionate and butyrate synthesis appear to be more species specific. Propionate is highly produced by gut microbes *Ruminococcus*, *Roseburia*, *Coprococcus*, *Clostridium*, *Megasphera*, *Veillonella*, *Dialister*, *Akkermansia*, and *Bacteroides* species (Reichardt et al., 2014). Butyrate is largely produced by *Faecalibacteria*, *Clostridia*, and *Roseburia* (Louis and Flint, 2009, 2017). Genome analysis suggests that other butyrate producers are members of *Actinobacteria*, *Bacteroidetes*, *Fusobacteria*, *Proteobacteria*, *Spirochaetes*, and *Thermotogae* (Vital et al., 2014). Many of these microbes are present in our SPF mice and, as a result, multiple strains could be working synergistically to generate the diverse range of neuro-active metabolites we observe *in vivo*. We think the fact that *B. ovatus* can generate many of the neuro-active compounds by itself is impressive. Particularly in the setting of an altered gut microbiota, *B. ovatus* administration may help elevate key neuro-active compounds. For example, in the setting of inflammatory bowel disease (IBD), where SCFA producing microbes are diminished, introduction of *B. ovatus* may elevate SCFAs acetate and propionate as well as branched SCFAs such as isobutryate and isovalerate. SCFA enemas are known to improve mucosal generation and improve symptoms in Ulcerative colitis patients (Jacobasch et al., 1999). Thus, *B. ovatus* administration may yield promising results.

An interesting finding from our work was that *in vitro B. ovatus* ATCC 8483 generated substantial tyramine and tyrosine, but *in vivo*, we observed no changes in these neurotransmitters. These findings suggest at least two possibilities. First, it is possible that *B. ovatus* produces tyramine and tyrosine *in vivo*, but these compounds are quickly taken up by the host. Tyramine can be transported into intestinal epithelial cells via OCT2 (Sarkar and Berry, 2020) and tyrosine can be taken up by L-Type Amino Acid Transporters (Fraga et al., 2002; Huang, 1965). These transporters are found in both mouse and human intestine. In the model organism *Caenorhabditis elegans*, commensal *Providencia* bacteria produce tyramine that then bypassed the requirement for the host to synthesize tyramine and manipulated host sensory decisions (O'Donnell et al., 2020). Similarly, *B. ovatus* produced tyramine and tyrosine could be absorbed by the intestinal epithelium of our gnotobiotic mice and thus prove to be undetected in our analysis. Another possibility is that our ZMB1 medium does not fully resemble the complex dynamic environment of the intestine. As a result, *B. ovatus* may behave differently in the intestine than our ZMB1 medium and may not generate tyramine and tyrosine.

Another noteworthy finding was that *B. ovatus* ATCC 8483 did not affect host serotonin levels. We speculate that this may be due in part to tryptophan levels. Our *in vitro* data indicate that *B. ovatus* consumes

tryptophan and our *in vivo* data indicate the *B. ovatus* mono-associated animals have lower intestinal tryptophan levels than germ-free mice. Our genome analysis and previously published data indicate that *B. ovatus* harbors the enzymatic machinery to generate indole-3-acetic acid (Ihekweazu et al., 2021). As a result, the conversion of tryptophan into indole-3-acetic acid may reduce tryptophan availability to the host, thereby limiting serotonin production. It should be noted that SPF mice also exhibit lower tryptophan levels than germ-free mice. Therefore, tryptophan bioavailability is not the only candidate. We have previously shown that unidentified microbial metabolites can stimulate enterochromaffin cells to synthesize and release serotonin in a dose-dependent manner (Engevik et al., 2021). We hypothesize that in SPF mice, microbes such as *Bacteroides* may be consuming tryptophan, whereas other microbes, such as *Bifidobacteria* and *Lactobacilli*, may be producing metabolites that activate enterochromaffin cells and promote serotonin production. Future work will need to be done to dissect which microbes and which corresponding metabolites activate the serotonin pathway.

Our genome analysis indicates that almost all *Bacteroides* species possess EC 2.7.2.7 and therefore should have the ability to generate butyrate. In contrast to our genome analysis, *B. ovatus* ATCC 8483 produced very little butyrate *in vitro* and no butyrate *in vivo*. Instead, we observed that *B. ovatus* produced isobutyric acid and 2-methyl-butyric acid. Branched SCFAs such as isobutyric acid and 2-methyl-butyric acid are produced during fermentation of branched chain amino acids (valine, leucine, and isoleucine) (Rios-Covian et al., 2020). It has been reported that the production of branched SCFAs in the gut is accomplished mainly by *Bacteroides* and *Clostridium* species (Aguirre et al., 2016; Rios-Covian et al., 2017; Smith and Macfarlane, 1998) and that branched SCFAs are produced in higher quantities when peptides are the main fuel source (Rios-Covian et al., 2020). Consistent with this notion, high-protein and low-complex carbohydrate diets, like the western diet, result in higher concentrations of branched SCFA *in vitro* and *in vivo* (Aguirre et al., 2016; Hald et al., 2016; Pieper et al., 2012). Moreover, the addition of complex carbohydrates or fiber consumption decreases fecal branched SCFA (François et al., 2014; Rios-Covian et al., 2020). Our ZMB1 contains valine (0.7 g/L), leucine (1.0 g/L), and isoleucine (0.24 g/L), as does our mouse chow (valine (w/w 0.91%), leucine (1.52%), and isoleucine (0.78%)). We speculate that the presence of these branched chain amino acids is likely driving the production of branched SCFAs by *B. ovatus in vitro* and *in vivo*. In the future, it would be interesting to see if elevating the levels of these branched amino acids could elevate *in vivo* levels of these branched SCFAs in *B. ovatus* mono-associated mice. It is possible that stable-label isotope tracing of the metabolic fate of carbon-13 labeled valine, leucine, and isoleucine in bacteria could provide some insights into the production of the branched SCFAs.

Traditionally, branched SCFAs have garnered significantly less attention than non-branched SCFAs, like acetate, propionate, and butyrate. However, branched SCFAs may be playing important roles in gut homeostasis. Isobutyrate stimulates colonic Na + absorption (Blachier et al., 2007) and serves as an energy source for colonocytes (Jaskiewicz et al., 1996). Additionally, small intestine development has been shown to be promoted by isovalerate (Liu et al., 2018) and branched SCFAs in general have been shown to regulate glucose and lipid metabolism (Heimann et al., 2016). Our study indicates that *B. ovatus* alone can generate the same branched SCFA profile as a complex gut microbiota and thus this gnotobiotic model with dietary manipulation could provide a valuable tool for dissecting the role of branched SCFAs in gut health.

It should be noted that our mouse chow contained substantial glutamate and nominal levels of tyrosine and tryptophan. Although our germ-free mice have provided a baseline of stool neuro-active compounds on this diet, we did not measure the amount of chow consumed by the mice. An increased consumption of a diet high in glutamate, tyrosine and tryptophan in our *B. ovatus* or SPF mice could influence the baseline levels of these neuro-active compounds and may provide an additional source for microbes. Other groups have found no difference in food consumption between age-matched germ-free and SPF mice (Bäckhed et al., 2007; Moretti et al., 2021). As a result, we speculate that food consumption may not be a large contributor in our study. However, future gnotobiotic studies should include analysis of food consumption to ensure that germ-free mice remain a good baseline for comparison.

The far-reaching effects of *Bacteroides* colonization has been demonstrated by two recent studies. Strandwitz et al. examined the human gut microbiota by 16S rRNA sequencing of stool samples of 23 patients who were clinically diagnosed with Major Depressive Disorder (MDD) and found that fecal *Bacteroides* relative abundance was inversely correlated with functional connectivity (indicative of depression) (Strandwitz et al., 2019). In another study, Tillisch et al. examined the gut microbiota of 40 healthy women and found that

Bacteroides levels were associated with increased gray matter in the cerebellum, hippocampus, and frontal regions of the brain (Tillisch et al., 2017). Additionally, these women exhibited reduced levels of anxiety, distress, and irritability in an emotional response test (Tillisch et al., 2017). In animal studies, a high fat diet has been shown to reduce *Bacteroides* levels and corresponded to reduced GABA levels in the prefrontal cortex, an affect that was associated with depressive-like behavior (Hassan et al., 2019). These studies provide a potential link between *Bacteroides*, GABA, and the gut-brain axis. In this study, we did not examine animal behavior, but we believe this is an important area of consideration for future work.

Collectively, this work characterizes the neuro-active metabolite profile associated with *B. ovatus* ATCC 8483. This study is unique in that we identified neuro-active compounds *in vitro* and linked them to *in vivo* levels. These findings point to *B. ovatus* ATCC 8483 as a neuro-modulating microbe and potentially a next-generation probiotic.

Limitations of the study

This study relied on feces and did not examine serum or neuronal neurotransmitter levels. Future work is necessary to determine the extent to which the feces reflect the neurotransmitter profiles of these compartments. Additionally, the examination of animal behavior would be necessary to confirm the functional significance of *B. ovatus* colonization.

STAR★METHODS

Detailed methods are provided in the online version of this paper and include the following:

- KEY RESOURCES TABLE
- RESOURCE AVAILABILITY
  - Lead contact
  - Materials availability
  - Data and code availability
- EXPERIMENTAL MODEL AND SUBJECT DETAILS
  - Bacterial culture
  - Mouse models
- METHOD DETAILS
  - Bacteroides genome mining
  - Generation of bacterial supernatant
  - Fecal collection and metabolite extraction procedures
  - 16S rRNA sequencing
  - LC-MS/MS equipment
  - LC-MS/MS method for glutamate cycle metabolites
  - LC-MS/MS method for the N-phenyl short-chain fatty acid (SCFA) derivatives
  - LC-MS/MS method for the quantitation of tryptophan pathway metabolites
  - LC-MS/MS method for the quantitation of tyrosine pathway metabolites
  - Metabolite networks
- QUANTIFICATION AND STATISTICAL ANALYSIS

ACKNOWLEDGMENTS

The Texas Children's Hospital Department of Pathology and Immunology provides salary support to Texas Children's Microbiome Center-Metabolomics Lab staff, and purchased all of the reagents, the consumables and durable supplies, and the LC-MS/MS equipment described.

AUTHOR CONTRIBUTIONS

Concept and design (T.D.H., F.D.A., A.M.H., J.V., M.A.E.); intellectual contribution (T.D.H., F.D.I., S.J.H., K.A.E., R.F., K.M.H., N.O., J.K.S., A.M.H., J.V., M.A.E.); data acquisition (T.D.H., F.D.I., S.J.H., K.A.E., R.F., K.M.H., M.A.E.); data analysis, statistics, and interpretation (T.D.H., F.D.I., S.J.H., K.M.H., N.O., J.K.S., A.M.H., M.A.E.); editing manuscript (T.D.H., F.D.I., S.J.H., K.A.E., R.F., K.M.H., N.O., J.K.S., A.M.H., J.V., M.A.E.); funding (F.D.I., A.M.H., J.V., M.A.E.).

DECLARATION OF INTERESTS

J.V. serves on the scientific advisory board of Seed, a USA-based probiotics/prebiotics company, Biomica, an Israeli informatics enterprise. and Plexus World-wide, a USA-based nutrition company. J.S.K. and J.V. receive unrestricted research support from BioGaia AB, a Swedish probiotics company. The remaining authors have no commercial or financial relationships to declare.

Received: February 8, 2021
Revised: November 1, 2021
Accepted: March 23, 2022
Published: May 20, 2022

REFERENCES

Aguirre, M., Eck, A., Koenen, M.E., Savelkoul, P.H.M., Budding, A.E., and Venema, K. (2016). Diet drives quick changes in the metabolic activity and composition of human gut microbiota in a validated in vitro gut model. Res. Microbiol. *167*, 114–125.

Bäckhed, F., Manchester, J.K., Semenkovich, C.F., and Gordon, J.I. (2007). Mechanisms underlying the resistance to diet-induced obesity in germ-free mice. Proc. Natl. Acad. Sci. U S A *104*, 979.

Barrett, E., Ross, R.P., O'Toole, P.W., Fitzgerald, G.F., and Stanton, C. (2012). gamma-Aminobutyric acid production by culturable bacteria from the human intestine. J. Appl. Microbiol. *113*, 411–417.

Bercik, P., Park, A.J., Sinclair, D., Khoshdel, A., Lu, J., Huang, X., Deng, Y., Blennerhassett, P.A., Fahnestock, M., Moine, D., et al. (2011). The anxiolytic effect of Bifidobacterium longum NCC3001 involves vagal pathways for gut-brain communication. Neurogastroenterol. Motil. *23*, 1132–1139.

Bercik, P., Collins, S.M., and Verdu, E.F. (2012). Microbes and the gut-brain axis. Neurogastroenterol. Motil. *24*, 405–413.

Blachier, F., Mariotti, F., Huneau, J.F., and Tome, D. (2007). Effects of amino acid-derived luminal metabolites on the colonic epithelium and physiopathological consequences. Amino Acids *33*, 547–562.

Caporaso, J.G., Kuczynski, J., Stombaugh, J., Bittinger, K., Bushman, F.D., Costello, E.K., Fierer, N., Pena, A.G., Goodrich, J.K., Gordon, J.I., et al. (2010). QIIME allows analysis of high-throughput community sequencing data. Nat. Methods *7*, 335–336.

Carabotti, M., Scirocco, A., Maselli, M.A., and Severi, C. (2015). The gut-brain axis: interactions between enteric microbiota, central and enteric nervous systems. Ann. Gastroenterol. *28*, 203–209.

Chen, C.Y., and Bonham, A.C. (2010). Postexercise hypotension: central mechanisms. Exerc. Sport Sci. Rev. *38*, 122–127.

Chen, I.M.A., Chu, K., Palaniappan, K., Ratner, A., Huang, J., Huntemann, M., Hajek, P., Ritter, S., Varghese, N., Seshadri, R., et al. (2021). The IMG/M data management and analysis system v.6.0: new tools and advanced capabilities. Nucleic Acids Res. *49*, D751–D763.

Clarke, G., Grenham, S., Scully, P., Fitzgerald, P., Moloney, R.D., Shanahan, F., Dinan, T.G., and Cryan, J.F. (2013). The microbiome-gut-brain axis during early life regulates the hippocampal serotonergic system in a sex-dependent manner. Mol. Psychiatry *18*, 666–673.

Cotter, P.D., Gahan, C.G., and Hill, C. (2001). A glutamate decarboxylase system protects Listeria monocytogenes in gastric fluid. Mol. Microbiol. *40*, 465–475.

Cryan, J.F., and Dinan, T.G. (2012). Mind-altering microorganisms: the impact of the gut microbiota on brain and behaviour. Nat. Rev. Neurosci. *13*, 701–712.

Cui, Y., Miao, K., Niyaphorn, S., and Qu, X. (2020). Production of gamma-aminobutyric acid from lactic acid bacteria: a systematic review. Int. J. Mol. Sci. *21*, 995.

De Vadder, F., Kovatcheva-Datchary, P., Goncalves, D., Vinera, J., Zitoun, C., Duchampt, A., Backhed, F., and Mithieux, G. (2014). Microbiota-generated metabolites promote metabolic benefits via gut-brain neural circuits. Cell *156*, 84–96.

Eckburg, P.B., Bik, E.M., Bernstein, C.N., Purdom, E., Dethlefsen, L., Sargent, M., Gill, S.R., Nelson, K.E., and Relman, D.A. (2005). Diversity of the human intestinal microbial flora. Science *308*, 1635–1638.

Engevik, M.A., and Versalovic, J. (2017). Biochemical features of beneficial microbes: foundations for therapeutic microbiology. Microbiol. Spectr. *5*. https://doi.org/10.1128/microbiolspec.BAD-0012-2016.

Engevik, M.A., Luck, B., Visuthranukul, C., Ihekweazu, F.D., Engevik, A.C., Shi, Z., Danhof, H.A., Chang-Graham, A.L., Hall, A., Endres, B.T., et al. (2021). Human-derived Bifidobacterium dentium modulates the mammalian serotonergic system and gut-brain axis. Cell. Mol. Gastroenterol. Hepatol. *11*, 221–248.

Feehily, C., and Karatzas, K.A. (2013). Role of glutamate metabolism in bacterial responses towards acid and other stresses. J. Appl. Microbiol. *114*, 11–24.

Fraga, S., Serrao, M.P., and Soares-da-Silva, P. (2002). L-type amino acid transporters in two intestinal epithelial cell lines function as exchangers with neutral amino acids. J. Nutr. *132*, 733–738.

François, I.E.J.A., Lescroart, O., Veraverbeke, W.S., Marzorati, M., Possemiers, S., Hamer, H., Windey, K., Welling, G.W., Delcour, J.A., Courtin, C.M., et al. (2014). Effects of wheat bran extract containing arabinoxylan oligosaccharides on gastrointestinal parameters in healthy preadolescent children. J. Pediatr. Gastroenterol. Nutr. *58*, 647–653.

Fujisaka, S., Avila-Pacheco, J., Soto, M., Kostic, A., Dreyfuss, J.M., Pan, H., Ussar, S., Altindis, E., Li, N., Bry, L., et al. (2018). Diet, genetics, and the gut microbiome drive dynamic changes in plasma metabolites. Cell Rep. *22*, 3072–3086.

Galland, L. (2014). The gut microbiome and the brain. J. Med. Food *17*, 1261–1272.

Gao, J., Xu, K., Liu, H., Liu, G., Bai, M., Peng, C., Li, T., and Yin, Y. (2018). Impact of the gut microbiota on intestinal immunity mediated by tryptophan metabolism. Front. Cell. Infect. Microbiol. *8*, 13.

Gill, R.K., Kumar, A., Malhotra, P., Maher, D., Singh, V., Dudeja, P.K., Alrefai, W., and Saksena, S. (2013). Regulation of intestinal serotonin transporter expression via epigenetic mechanisms: role of HDAC2. Am. J. Physiol. Cell Physiol. *304*, C334–C341.

Hald, S., Schioldan, A.G., Moore, M.E., Dige, A., Laerke, H.N., Agnholt, J., Bach Knudsen, K.E., Hermansen, K., Marco, M.L., Gregersen, S., et al. (2016). Effects of arabinoxylan and resistant starch on intestinal microbiota and short-chain fatty acids in subjects with metabolic syndrome: a randomised crossover study. PLoS One *11*, e0159223.

Hassan, A.M., Mancano, G., Kashofer, K., Frohlich, E.E., Matak, A., Mayerhofer, R., Reichmann, F., Olivares, M., Neyrinck, A.M., Delzenne, N.M., et al. (2019). High-fat diet induces depression-like behaviour in mice associated with changes in microbiome, neuropeptide Y, and brain metabolome. Nutr. Neurosci. *22*, 877–893.

Heimann, E., Nyman, M., Pålbrink, A.-K., Lindkvist-Petersson, K., and Degerman, E. (2016). Branched short-chain fatty acids modulate glucose and lipid metabolism in primary adipocytes. Adipocyte *5*, 359–368.

Hildebrand, F., Tadeo, R., Voigt, A.Y., Bork, P., and Raes, J. (2014). LotuS: an efficient and user-friendly OTU processing pipeline. Microbiome *2*, 30.

Hoyles, L., Snelling, T., Umlai, U.K., Nicholson, J.K., Carding, S.R., Glen, R.C., and McArthur, S. (2018). Microbiome-host systems interactions: protective effects of propionate upon the blood-brain barrier. Microbiome *6*, 55.

Huang, K.C. (1965). Uptake of L-tyrosine and 3-0-methylglucose by isolated intestinal epithelial cells. Life Sci. *4*, 1201–1206.

Hyland, N.P., and Cryan, J.F. (2010). A gut feeling about GABA: focus on GABA(B) receptors. Front. Pharmacol. *1*, 124.

Ihekweazu, F.D., Fofanova, T.Y., Queliza, K., Nagy-Szakal, D., Stewart, C.J., Engevik, M.A., Hulten, K.G., Tatevian, N., Graham, D.Y., Versalovic, J., et al. (2019). Bacteroides ovatus ATCC 8483 monotherapy is superior to traditional fecal transplant and multi-strain bacteriotherapy in a murine colitis model. Gut Microbes *10*, 504–520.

Ihekweazu, F.D., Engevik, M.A., Ruan, W., Shi, Z., Fultz, R., Engevik, K.A., Chang-Graham, A.L., Freeborn, J., Park, E.S., Venable, S., et al. (2021). Bacteroides ovatus promotes IL-22 production and reduces trinitrobenzene sulfonic acid (TNBS)-driven colonic inflammation. Am. J. Pathol. *191*, 704–719.

Jacobasch, G., Schmiedl, D., Kruschewski, M., and Schmehl, K. (1999). Dietary resistant starch and chronic inflammatory bowel diseases. Int. J. Colorectal Dis. *14*, 201–211.

Jaskiewicz, J., Zhao, Y., Hawes, J.W., Shimomura, Y., Crabb, D.W., and Harris, R.A. (1996). Catabolism of isobutyrate by colonocytes. Arch. Biochem. Biophys. *327*, 265–270.

Jin, Z., Mendu, S.K., and Birnir, B. (2013). GABA is an effective immunomodulatory molecule. Amino Acids *45*, 87–94.

Langmead, B., and Salzberg, S.L. (2012). Fast gapped-read alignment with Bowtie 2. Nat. Methods *9*, 357–359.

Ley, R.E., Backhed, F., Turnbaugh, P., Lozupone, C.A., Knight, R.D., and Gordon, J.I. (2005). Obesity alters gut microbial ecology. Proc. Natl. Acad. Sci. U S A *102*, 11070–11075.

Ley, R.E., Turnbaugh, P.J., Klein, S., and Gordon, J.I. (2006). Microbial ecology: human gut microbes associated with obesity. Nature *444*, 1022–1023.

Liu, Q., Wang, C., Zhang, Y.L., Pei, C.X., Zhang, S.L., Guo, G., Huo, W.J., and Yang, W.Z. (2018). Effects of isovalerate supplementation on morphology and functional gene expression of small intestine mucosa in pre- and post-weaned dairy calves. J. Agric. Sci. *156*, 272–281.

Louis, P., and Flint, H.J. (2009). Diversity, metabolism and microbial ecology of butyrate-producing bacteria from the human large intestine. FEMS Microbiol. Lett. *294*, 1–8.

Louis, P., and Flint, H.J. (2017). Formation of propionate and butyrate by the human colonic microbiota. Environ. Microbiol. *19*, 29–41.

Luck, B., Engevik, M.A., Ganesh, B.P., Lackey, E.P., Lin, T., Balderas, M., Major, A., Runge, J., Luna, R.A., Sillitoe, R.V., et al. (2020). Bifidobacteria shape host neural circuits during postnatal development by promoting synapse formation and microglial function. Sci. Rep. *10*, 7737.

Luk, B., Veeraragavan, S., Engevik, M., Balderas, M., Major, A., Runge, J., Luna, R.A., and Versalovic, J. (2018). Postnatal colonization with human "infant-type" Bifidobacterium species alters behavior of adult gnotobiotic mice. PLoS One *13*, e0196510.

Ma, N., and Ma, X. (2019). Dietary amino acids and the gut-microbiome-immune Axis: physiological metabolism and therapeutic prospects. Compr. Rev. Food Sci. Food Saf. *18*, 221–242.

Martin, C.R., Osadchiy, V., Kalani, A., and Mayer, E.A. (2018). The brain-gut-microbiome axis. Cell. Mol. Gastroenterol. Hepatol. *6*, 133–148.

Matsumoto, M., Ooga, T., Kibe, R., Aiba, Y., Koga, Y., and Benno, Y. (2017). Colonic absorption of low-molecular-weight metabolites influenced by the intestinal microbiome: a pilot study. PLoS One *12*, e0169207.

Moretti, C.H., Schiffer, T.A., Li, X., Weitzberg, E., Carlström, M., and Lundberg, J.O. (2021). Germ-free mice are not protected against diet-induced obesity and metabolic dysfunction. Acta Physiol. (Oxf) *231*, e13581.

Morrison, D.J., and Preston, T. (2016). Formation of short chain fatty acids by the gut microbiota and their impact on human metabolism. Gut Microbes *7*, 189–200.

Ney, D.M., Murali, S.G., Stroup, B.M., Nair, N., Sawin, E.A., Rohr, F., and Levy, H.L. (2017). Metabolomic changes demonstrate reduced bioavailability of tyrosine and altered metabolism of tryptophan via the kynurenine pathway with ingestion of medical foods in phenylketonuria. Mol. Genet. Metab. *121*, 96–103.

Nguyen, T.L., Vieira-Silva, S., Liston, A., and Raes, J. (2015). How informative is the mouse for human gut microbiota research? Dis. Model Mech. *8*, 1–16.

Nohr, M.K., Pedersen, M.H., Gille, A., Egerod, K.L., Engelstoft, M.S., Husted, A.S., Sichlau, R.M., Grunddal, K.V., Poulsen, S.S., Han, S., et al. (2013). GPR41/FFAR3 and GPR43/FFAR2 as cosensors for short-chain fatty acids in enteroendocrine cells vs FFAR3 in enteric neurons and FFAR2 in enteric leukocytes. Endocrinology *154*, 3552–3564.

O'Donnell, M.P., Fox, B.W., Chao, P.H., Schroeder, F.C., and Sengupta, P. (2020). A neurotransmitter produced by gut bacteria modulates host sensory behaviour. Nature *583*, 415–420.

O'Mahony, S.M., Clarke, G., Borre, Y.E., Dinan, T.G., and Cryan, J.F. (2015). Serotonin, tryptophan metabolism and the brain-gut-microbiome axis. Behav. Brain Res. *277*, 32–48.

Park, J.S., Lee, E.J., Lee, J.C., Kim, W.K., and Kim, H.S. (2007). Anti-inflammatory effects of short chain fatty acids in IFN-gamma-stimulated RAW 264.7 murine macrophage cells: involvement of NF-kappaB and ERK signaling pathways. Int. Immunopharmacol. *7*, 70–77.

Park, J., Kim, M., Kang, S.G., Jannasch, A.H., Cooper, B., Patterson, J., and Kim, C.H. (2015). Short-chain fatty acids induce both effector and regulatory T cells by suppression of histone deacetylases and regulation of the mTOR-S6K pathway. Mucosal Immunol. *8*, 80–93.

Park, J.H., Kotani, T., Konno, T., Setiawan, J., Kitamura, Y., Imada, S., Usui, Y., Hatano, N., Shinohara, M., Saito, Y., et al. (2016). Promotion of intestinal epithelial cell turnover by commensal bacteria: role of short-chain fatty acids. PLoS One *11*, e0156334.

Park, J., Wang, Q., Wu, Q., Mao-Draayer, Y., and Kim, C.H. (2019a). Bidirectional regulatory potentials of short-chain fatty acids and their G-protein-coupled receptors in autoimmune neuroinflammation. Sci. Rep. *9*, 8837.

Park, J.W., Kim, H.Y., Kim, M.G., Jeong, S., Yun, C.H., and Han, S.H. (2019b). Short-chain fatty acids inhibit staphylococcal lipoprotein-induced nitric oxide production in murine macrophages. Immune Netw. *19*, e9.

Pieper, R., Kröger, S., Richter, J.F., Wang, J., Martin, L., Bindelle, J., Htoo, J.K., von Smolinski, D., Vahjen, W., Zentek, J., et al. (2012). Fermentable fiber ameliorates fermentable protein-induced changes in microbial ecology, but not the mucosal response, in the colon of piglets. J. Nutr. *142*, 661–667.

Pokusaeva, K., Johnson, C., Luk, B., Uribe, G., Fu, Y., Oezguen, N., Matsunami, R.K., Lugo, M., Major, A., Mori-Akiyama, Y., et al. (2017). GABA-producing Bifidobacterium dentium modulates visceral sensitivity in the intestine. Neurogastroenterol. Motil. *29*, e12904.

Quast, C., Pruesse, E., Yilmaz, P., Gerken, J., Schweer, T., Yarza, P., Peplies, J., and Glockner, F.O. (2013). The SILVA ribosomal RNA gene database project: improved data processing and web-based tools. Nucleic Acids Res. *41*, D590–D596.

Reichardt, N., Duncan, S.H., Young, P., Belenguer, A., McWilliam Leitch, C., Scott, K.P., Flint, H.J., and Louis, P. (2014). Phylogenetic distribution of three pathways for propionate production within the human gut microbiota. ISME J. *8*, 1323–1335.

Rios-Covian, D., Salazar, N., Gueimonde, M., and de los Reyes-Gavilan, C.G. (2017). Shaping the metabolism of intestinal Bacteroides population through diet to improve human health. Front. Microbiol. *8*, 376.

Rios-Covian, D., González, S., Nogacka, A.M., Arboleya, S., Salazar, N., Gueimonde, M., and de los Reyes-Gavilán, C.G. (2020). An overview on fecal branched short-chain fatty acids along human life and as related with body mass index: associated dietary and anthropometric factors. Front. Microbiol. *11*, 973.

Sanders, J.W., Leenhouts, K., Burghoorn, J., Brands, J.R., Venema, G., and Kok, J. (1998). A chloride-inducible acid resistance mechanism in *Lactococcus lactis* and its regulation. Mol. Microbiol. *27*, 299–310.

Sarkar, S., and Berry, M.D. (2020). Involvement of organic cation transporter 2 and a Na(+)-dependent active transporter in p-tyramine

transport across Caco-2 intestinal cells. Life Sci. *253*, 117696.

Shannon, P., Markiel, A., Ozier, O., Baliga, N.S., Wang, J.T., Ramage, D., Amin, N., Schwikowski, B., and Ideker, T. (2003). Cytoscape: a software environment for integrated models of biomolecular interaction networks. Genome Res. *13*, 2498–2504.

Small, P.L., and Waterman, S.R. (1998). Acid stress, anaerobiosis and *gadCB*: lessons from *Lactococcus lactis* and *Escherichia coli*. Trends Microbiol. *6*, 214–216.

Smith, E.A., and Macfarlane, G.T. (1998). Enumeration of amino acid fermenting bacteria in the human large intestine: effects of pH and starch on peptide metabolism and dissimilation of amino acids. FEMS Microbiol. Ecol. *25*, 355–368.

Stefanko, D.P., Barrett, R.M., Ly, A.R., Reolon, G.K., and Wood, M.A. (2009). Modulation of long-term memory for object recognition via HDAC inhibition. Proc. Natl. Acad. Sci. U S A *106*, 9447–9452.

Strandwitz, P., Kim, K.H., Terekhova, D., Liu, J.K., Sharma, A., Levering, J., McDonald, D., Dietrich, D., Ramadhar, T.R., Lekbua, A., et al. (2019). GABA-modulating bacteria of the human gut microbiota. Nat. Microbiol. *4*, 396–403.

Su, M.S., Schlicht, S., and Ganzle, M.G. (2011). Contribution of glutamate decarboxylase in *Lactobacillus reuteri* to acid resistance and persistence in sourdough fermentation. Microb. Cell Fact. *10*, S8.

Sze, P.Y. (1979). L-Glutamate decarboxylase. Adv. Exp. Med. Biol. *123*, 59–78.

Tan, H., Yu, Z., Wang, C., Zhang, Q., Zhao, J., Zhang, H., Zhai, Q., and Chen, W. (2018). Pilot safety evaluation of a novel strain of Bacteroides ovatus. Front. Genet. *9*, 539.

Tillisch, K., Mayer, E.A., Gupta, A., Gill, Z., Brazeilles, R., Le Neve, B., van Hylckama Vlieg, J.E.T., Guyonnet, D., Derrien, M., and Labus, J.S. (2017). Brain structure and response to emotional stimuli as related to gut microbial profiles in healthy women. Psychosom. Med. *79*, 905–913.

Vecsey, C.G., Hawk, J.D., Lattal, K.M., Stein, J.M., Fabian, S.A., Attner, M.A., Cabrera, S.M., McDonough, C.B., Brindle, P.K., Abel, T., et al. (2007). Histone deacetylase inhibitors enhance memory and synaptic plasticity via CREB:CBP-dependent transcriptional activation. J. Neurosci. *27*, 6128–6140.

Vital, M., Howe, A.C., and Tiedje, J.M. (2014). Revealing the bacterial butyrate synthesis pathways by analyzing (meta)genomic data. mBio *5*, e00889.

Waclawikova, B., and El Aidy, S. (2018). Role of microbiota and tryptophan metabolites in the remote effect of intestinal inflammation on brain and depression. Pharmaceuticals (Basel) *11*, 63.

Wang, Q., Garrity, G.M., Tiedje, J.M., and Cole, J.R. (2007). Naive Bayesian classifier for rapid assignment of rRNA sequences into the new bacterial taxonomy. Appl. Environ. Microbiol. *73*, 5261–5267.

Wexler, H.M. (2007). Bacteroides: the good, the bad, and the nitty-gritty. Clin. Microbiol. Rev. *20*, 593–621.

Williams, B.B., Van Benschoten, A.H., Cimermancic, P., Donia, M.S., Zimmermann, M., Taketani, M., Ishihara, A., Kashyap, P.C., Fraser, J.S., and Fischbach, M.A. (2014). Discovery and characterization of gut microbiota decarboxylases that can produce the neurotransmitter tryptamine. Cell Host Microbe *16*, 495–503.

Wong, C.G., Bottiglieri, T., and Snead, O.C., 3rd (2003). GABA, gamma-hydroxybutyric acid, and neurological disease. Ann. Neurol. *54*, S3–S12.

Zhang, G., Mills, D.A., and Block, D.E. (2009). Development of chemically defined media supporting high-cell-density growth of lactococci, enterococci, and streptococci. Appl. Environ. Microbiol. *75*, 1080–1087.

STAR★METHODS

KEY RESOURCES TABLE

REAGENT or RESOURCE	SOURCE	IDENTIFIER
Bacterial and virus strains		
Bacteroides ovatus	ATCC	8483
Chemicals, peptides, and recombinant proteins		
BD Difco Brain-heart-infusion Broth	Fisher Scientific	DF0037-17-8
BD Difco Brain-heart-infusion Agar	Fisher Scientific	DF0418-15-9
Yeast extract	Fisher Scientific	BP1422-500
Cysteine	Fisher Scientific	C051625G
PBS	Fisher Scientific	BP665-1
Optima™ LC/MS-grade water	Fisher Scientific	W6-4
Optima™ LC/MS-grade acetonitrile (ACN)	Fisher Scientific	A955-4
Optima™ LC/MS-grade methanol	Fisher Scientific	A456-4
Optima™ LC/MS-grade acetic acid	Fisher Scientific	A11350
Optima™ LC/MS-grade formic acid (FA)	Fisher Scientific	A117-50
LC-MS-grade LiChropur™ ammonium acetate	Millipore-Sigma	73594
LC-MS-grade LiChropur™ ammonium formate	Millipore-Sigma	70221
ion-chromatography-grade heptafluorobutyric acid (HFBA)	Millipore-Sigma	52411-25ML-F
L-glutamine	Millipore-Sigma	G3126
L-glutamate	Millipore-Sigma	G1251
GABA	Millipore-Sigma	A2129
d5-L-glutamate	Millipore-Sigma	616281
d6-GABA	Millipore-Sigma	615587
d5-L-glutamine	CDN Isotopes	D-2532
L-tryptophan (Trp)	Fisher Scientific	AC140590250
5-hydroxy-L-tryptophan (5-OH-Trp)	Fisher Scientific	H05311G
serotonin	Fisher Scientific	AC215025000
melatonin	Fisher Scientific	ICN10225401
N-acetylserotonin	Millipore-Sigma	A1824
5-hydroxyindoleacetic acid (5-HIAA)	Millipore-Sigma	H8876
tryptamine	Millipore-Sigma	246557
d5-L-Trp	CDN isotopes	D-1522
d3-5-OH-Trp	CDN isotopes	D-7154
d4-melatonin	CDN isotopes	D-2952
d5-HIAA	CDN isotopes	D-6725
d4-serotonin	Santa Cruz Biotechnology	sc-473411
anthranilic acid	Millipore-Sigma	10680
dopamine	Millipore-Sigma	H8502
epinephrine	Millipore-Sigma	E4250
levodopa (L-DOPA)	Millipore-Sigma	D9628
D,L-norepinephrine	Millipore-Sigma	A7256
L-tyrosine (Tyr)	Millipore-Sigma	T3754
L-tyramine	Fisher Scientific	AC140610250

(*Continued on next page*)

Continued

REAGENT or RESOURCE	SOURCE	IDENTIFIER
d4-dopamine	Millipore-Sigma	655651
d6-epinephrine	Millipore-Sigma	E-077
d3-L-DOPA	Millipore-Sigma	333786
d4-L-tyramine	Santa Cruz Biotechnology	sc-220347
propionic acid	Millipore-Sigma	402907
isobutyric acid	Millipore-Sigma	I1754
butyric acid	Millipore-Sigma	B103500
2-methylbutyric acid	Millipore-Sigma	W269514
isovaleric acid	Millipore-Sigma	129542
valeric acid	Millipore-Sigma	240370
aniline	Millipore-Sigma	132934
[$^{13}C_6$]-aniline	Millipore-Sigma	485497
1-(3-dimethylaminopropyl)-3-ethylcarbodiimide hydrochloride (EDAC)	Fisher Scientific	03450
2-mercaptoethanol	Fisher Scientific	AC125470100
succinic acid	Fisher Scientific	AC158742500
Deposited data		
16S Sequencing	This paper	PRJNA788494
Experimental models: Cell lines		
Germ-free Swiss Webster Mice	BCM Colony	024
Select Rodent 50 IF/6F auto 5V0F chow	Lab Diet.com	3002875-703
Other		
Viva BiPh Biphenyl (100 mm x 1 mm, 5 µm, 300 Å pore size) analytical column	Restek	9516511
Viva BiPh Biphenyl (10 mm x 2.1 mm, 5 µm, 300 Å pore size) guard cartridge	Restek	951650212
Supelco Ascentis® Express HILIC (150 mm x 2.1 mm, 2.7 µm, 90 Å pore) analytical column	Millipore-Sigma	53946-U
Luna C18(2) (150 mm x 1 mm, 3 µm, 100 Å pore size) analytical column	Phenomenex	00F-4251-A0
C18 SecurityGuard™ (4 mm x 2 mm) cartridge	Phenomenex	AJO-4286
Raptor C18 (100 mm x 1 mm, 2.7 µm, 90 Å pore size) analytical column	Restek	9304A12
Ultra C18 (10 mm x 2.1 mm, 5 µm, 100 Å pore size) guard cartridge	Restek	917450212
Software and algorithms		
Sciex Analyst®	Danaher	Version 1.6.2
Sciex MultiQuant™	Danaher	Version 3.0.6256.0
Prism	Graphpad	Version 9.3
Cytoscape	https://cytoscape.org/	Version 3.8.2
Python	www.python.org	Version 3.8
Spyder	www.Spyder-ide.org	Version 4.2.5
Other		
Nexera-XR MP UPHLC system	Shimadzu	www.shimadzu.com
Sciex 6500 QTRAP hybrid triple-quadrupole/ linear ion trap mass spectrometer	Danaher	https://sciex.com

RESOURCE AVAILABILITY

Lead contact

Further information and requests for resources and reagents should be directed to and will be fulfilled by the lead contact, Melinda A. Engevik at engevik@musc.edu.

Materials availability

This study did not generate new unique reagents.

Data and code availability

- The 16S rRNA data have been deposited at BioProject under the project ID PRJNA788494 at: https://urldefense.proofpoint.com/v2/url?u=http-3A__www.ncbi.nlm.nih.gov_bioproject_788494&d=DwICaQ&c=ZQs-KZ8oxEw0p81sqgiaRA&r=LoElyxtsmT0qK5iTKwenmw&m=ZoKnKXUppxX9TDAWS52PiQX__rSEBaqHu_wu8xgqHG3O_SSRlRRpRFTwkA-4kLO_&s=uPXCYJYKhXUAQHNfASTzKo9QFsfZSuTqREOc3Ee5fwY&e=.
- No original code was generated
- All data reported in this paper will be shared by the lead contact upon request. This paper does not report original code.

EXPERIMENTAL MODEL AND SUBJECT DETAILS

Bacterial culture

Bacteroides ovatus ATCC 8483 (ATCC, American Type Culture Collection) was cultured in Brain-Heart-Infusion medium (Difco) supplemented with 2% yeast extract, and 0.2% cysteine (BHIS) in an anaerobic workstation (Anaerobe Systems AS-580) at 37°C with a gas mixture of 5% CO_2, 5% H_2, and 90% N_2. For gnotobiotic experiments, *B. ovatus* was grown in BHIS anaerobically overnight, centrifuged at 5,000 × *g* for 5 min and washed twice with sterile anaerobic PBS to remove residual BHIS and adjusted to 2×10^8 cells mL^{-1} in sterile anaerobic PBS. This bacterial suspension was used for oral gavage of germ-free mice. Bacterial viability was confirmed by serially plating *B. ovatus* on BHIS agar.

Mouse models

Germ-free and gnotobiotic experimental procedures were approved by the Institutional Animal Care and Use Committee (IACUC) at Baylor College of Medicine, Houston, TX. Gnotobiotic mouse experiments were performed in sterile isolators in the Baylor College of Medicine germ-free facility. Mice consumed sterile Select Rodent 50 IF/6F auto 5V0F chow (cat# 3002875-703, Lab Diet.com), which contains which contains w/w 0.58% tyrosine, 0.23% tryptophan, and 4.41% glutamic acid (glutamate). Animals were randomly assigned to experimental groups. Germ-free Swiss-Webster male mice at 8–12 weeks old were gavaged with sterile PBS (germ-free controls) or 2×10^8 CFU mL^{-1} *B. ovatus* ATCC 8483 in PBS (*B. ovatus* mono-associated). Mice received oral gavages once every other day for one week and one final gavage a week later. Mice were maintained in isolators for 17 days. Colonization was confirmed by culturing fecal samples from mice prior to treatment and 17 days after treatment on BHIS agar plates (Hardy Diagnostics) anaerobically at 37°C. Specific pathogen free (SPF) Swiss-Webster male mice, harboring a complete gut microbiota since birth, were age-matched and used as controls for *in vivo* analysis.

METHOD DETAILS

Bacteroides genome mining

The ability of *Bacteroides* members to generate neuro-active metabolites was estimated using the Integrated Microbial Genomes (IMG) database v5.0 (http://img.jgi.doe.gov) (Chen et al., 2021). The pipeline used by this database annotates publicly available sequence data using several common function prediction tools (including Pfam, Inter-Pro domains, and KEGG Ortholog terms/pathways, among others), and combines these records for individual genes and genomes. The Enzyme Commission numbers (ECs) for the enzymes involved in neuro-active compound production were identified in *Bacteroides* using the KEGG database (KEGG: Kyoto Encyclopedia of Genes and Genomes, https://www.genome.jp). ECs were input into the gene search tool of the IMG database and the Bacteroides genomes were binned for analysis. Search terms included EC 1.2.1.16, EC 2.6.1.19, EC 6.3.1.2, EC 1.4.1.13, EC 5.4.99.5, EC

1.3.1.12, EC 2.6.1.1, EC 4.1.1.11, EC 1.2.7.1, EC 2.7.2.1, EC 1.2.7.11, EC 6.2.1.1 and EC 2.7.2.7. Resulting genomes used in the analysis are shown in Table 1.

Generation of bacterial supernatant

Bacteroides ovatus ATCC 8483 was cultured in BHIS overnight anaerobically at 37°C. After culturing in BHIS, *B. ovatus* was sub-cultured into a chemically defined medium, termed ZMB1 (Zhang et al., 2009), at an optical density (OD_{600nm}) = 0.1 and cultured anaerobically at 37°C for 18 h. Cultures were centrifuged at 5,000 × *g* for 5 min and the supernatants were sterile-filtered through a 0.2 μm-pore PVDF-membrane (Polyvinylidene Fluoride, Millipore). Samples were stored frozen at −80°C until the metabolomic method could be performed.

Fecal collection and metabolite extraction procedures

Fecal samples were collected from all mice before euthanasia. For metabolite extraction, an ~50 mg mass of each stool sample was weighed, mixed at a fecal material density of 0.1 mg/μL in ice-cold ACN:water (1:1, *v/v*), homogenized by vortex-mixing for 5 min, centrifuged at 16,000 *x g* for 5 min, and the supernatant of the stool sample extract was transferred to a new tube and was stored frozen at −80°C prior to downstream processing. The stool sample masses and extraction solvent volumes were recorded for downstream metabolite concentration normalizations.

Prior to starting, an extraction solvent consisting of acetonitrile:water (1:1, *v,v*) was chilled in a wet-ice batch for a minimum period of 1 h. A targeted mass of 50 mg of stool pellets were placed into 1.5 mL Eppendorf tubes and weighed, and the wet mass of each stool sample was recorded for metabolite normalization purposes. An extraction solvent volume equivalent to a stool density of 0.1 mg/μL was added to each sample, and the samples were vortex-mixed with a multitube vortexer for 5 min to homogenize the fecal solids. If needed, samples were briefly sonicated to disperse large chunks of feces. Stool sample debris was pelleted by centrifugation at 16,000*g* for 5 min. The stool sample supernatant extract was placed into a new tube and was stored frozen at −80°C until the metabolomic method could be performed.

16S rRNA sequencing

The intestinal microbial composition was examined from fecal samples by 16S sequencing. The MoBio Powersoil DNA Extraction Kit (Qiagen) was used to isolate bacterial DNA, which was sequenced by the Texas Children's Microbiome Center (Luk et al., 2018). Briefly, NEXTflex™ 16S V4 Amplicon-Seq Kit 2.0 (Bioo Scientific, Austin, TX) was used to generate gene sequence libraries (targeting the V4 region of the 16S rRNA gene). These libraries were sequenced on the Illumina MiSeq platform (median of 24,181 sequences/sample, mean of 25,801 sequences/sample). Bowtie2 was used to filter out host (mouse) DNA sequences from the sequence libraries and sequencing reads were filtered for quality using LotuS (Hildebrand et al., 2014; Langmead and Salzberg, 2012). After quality filtering sequences, reads were pair-end stitched and resulting sequences were clustered (with a 97% similarity level threshold) into operational taxonomic units (OTUs) using LotuS with the Ribosomal Database Project Classifier (Wang et al., 2007). To assign taxonomy, the Ribosomal Database Project Classifier trained on the SILVA v123 reference database (Quast et al., 2013) was used. Bacterial community profiles were then analyzed using QIIME v1.9 (Caporaso et al., 2010). Output sequences were classified at the phylum and genus levels for comparisons. Germ-free mice and *B. ovatus* mice were examined by qPCR with a Universal bacterial primer and *B. ovatus*-specific primers (Ihekweazu et al., 2021).

LC-MS/MS equipment

The liquid chromatography-tandem mass spectrometry (LC-MS/MS) system was comprised of a Shimadzu Nexera X2 MP Ultrahigh-Performance Liquid Chromatography (UHPLC) system (Kyoto, Japan) coupled to a Sciex 6500 QTrap hybrid triple-quadrupole/linear ion trap MS system from Danaher (Washington, DC, USA). Operational control of the LC-MS/MS was performed with Analyst® (Ver. 1.6.2), and quantitative analysis was performed using MultiQuant™ (Ver. 3.0.6256.0).

LC-MS/MS method for glutamate cycle metabolites

Internal Standard (IS) stock solutions for d5-glutamate, d5-glutamine, and d6-GABA were each prepared at 10.0 mg/mL in water. An IS Solution-A (ISS-A) was prepared from each of the IS stocks at a concentration of 500 ng/mL for each in a solution of acetonitrile:water (9:1, *v:v*) and 0.1% formic acid; the ISS-A solution was

used in the final preparation of the microbiome samples. An ISS-B solution was prepared at a concentration of 450 ng/mL for each deuterated internal standard compound by diluting 9 mL of the ISS-A solution with 1 mL of acetonitrile:water (9:1, *v:v*) and 0.1% formic acid; This solution was used to prepare the combined intermediate solution and the Calibration Standards (Calibrators).

Stock solutions for glutamate, glutamine, and GABA were each prepared at 10.0 mg/mL in water. A combined intermediate was prepared from each of the stocks at a concentrations of 100 μg/mL for each using Glutamate Cycle ISS-B as the diluent. Calibrators were prepared from the combined intermediate by serial dilution (DF 4-fold per Calibrator level) at metabolite concentrations of 1,000, 250, 62.5, 15.6, 3.90, and 0.977 ng/mL using Glutamate Cycle ISS-B as the diluent.

Stool sample extracts were thawed on the benchtop at ambient room temperature, and were vortex-mixed briefly. A 10-μL volume of stool sample extract was diluted in a 90-μL volume of the Glutamate Cycle ISS-A solution directly in an autosampler vial, and the 10-fold diluted sample was vortex-mixed for 30 s. The samples were transferred to an autosampler and a 5-μL sample volume was injected onto the LC-MS/MS system for analysis.

The Glutamate Cycle method uses hydrophilic interaction chromatography (HILIC) separation for the measurement of the glutamate, glutamine, and GABA. Chemical separations were performed using a mobile phase A (MPA) solution consisting of ACN:water (9:1, *v:v*) and 10 mM ammonium formate and 2% FA, a mobile phase B (MPB) solution consisting of ACN:water (1:1, *v:v*) and 10 mM ammonium formate and 2% FA, and a needlewash solution (NW) consisting of ACN:water (1:1, *v:v*). Chromatographic separations were performed using an Ascentis® Express HILIC (150 mm × 2.1 mm, 2.7 μm) analytical column. The mobile phase flowrate was 0.200 mL/min, the autosampler trays were chilled to 4°C, the column oven was heated at 30°C, and the gradient elution program used was 0-2.5 min, 0% MPB; 2.5–10.5 min, 0–50% MPB; 10.5–13.0 min, 50% MPB; 13.0–14.0 min, 50-0% MPB; 14.0–17.0 min, 0% MPB with a gradient cycle time of 17.4 min per sample. A TurboIonSpray® electrospray ionization (ESI) probe was installed and the 6500 QTrap MS was operated in positive ionization mode using a selected-reaction monitoring (SRM) scan mode under the following instrumental conditions: IonSpray voltage of +5,000 volts (V); Curtain gas (Cur): 20 psi; Temperature (Temp): 200°C; Source Gas 1 (GS1): 25 psi; Source Gas 2 (GS2): 25 psi; Collisionally-activated dissociation (CAD) gas: HIGH; and the Q1 and Q3 quadruple resolution settings were set to Unit/Unit. See Table 2 for the metabolite specific SRM transition parameters for the glutamate cycle metabolites.

LC-MS/MS method for the N-phenyl short-chain fatty acid (SCFA) derivatives

The derivatization procedure used to synthesize the [$^{13}C_6$]-N-phenyl SCFA IS standard derivatives, the non-labeled N-phenyl SCFA analyte standard derivatives, the stock and intermediate solutions, and the calibration standard preparations have all been described previously (Engevik et al., 2021). The linear dynamic range for the assay is from 9.77 nM to 10,000 nM for each of the N-phenyl SCFA derivatized analytes. The reverse-phase separation for the measurement of N-phenyl SCFA derivatives was performed using an MPA solution consisting of water:FA (99.9:0.1, *v:v*), a MPB solution consisting of methanol:FA (99.9:0.1, *v:v*), and a NW consisting of methanol:water (1:1, *v:v*). Chromatographic separations were performed using a Viva BiPh Biphenyl (100 mm × 1 mm, 5 μm) analytical column equipped with a Viva Bi-Ph Biphenyl (10 mm × 2.1 mm, 5 μm) guard cartridge. The mobile phase flowrate was 0.200 mL/min, the autosampler trays were chilled to 10°C, the column oven was heated at 50°C, and the gradient elution program used was 0-2.0 min, 5% MPB; 2.0–9.0 min, 5–50% MPB; 9.0–9.1 min, 50-5% MPB; 9.1–12.0 min, 5% MPB with a gradient cycle time of 12.4 min per sample. An ESI probe was installed and the 6500 QTrap MS was operated in positive ionization mode using an SRM scan mode with the following instrumental conditions: IonSpray voltage of +5,000 V; Cur: 20 psi; Temp: 200°C; GS1/GS2: 25 psi each; CAD gas: HIGH; and, Q1/Q3 resolution: Unit/Unit. See Table 3 for the metabolite specific SRM transition parameters for the SCFAs.

LC-MS/MS method for the quantitation of tryptophan pathway metabolites

IS stock solutions for d5-5-hydroxyindoleacetic acid (5-HIAA), d3-5-hydroxytryptophan, d4-melatonin, d4-serotonin, and d5-tryptophan were each prepared at 10.0 mg/mL in water. An ISS-A solution was prepared from each of the IS stocks at a concentration of 500 ng/mL each for d5-tryptophan, d4-serotonin, and d4-melatonin, and 1,500 ng/mL for d5-HIAA in water; the ISS-A solution was used in the final preparation of the microbiome samples. An ISS-B solution was prepared at a concentration of 450 ng/mL each for d5-tryptophan, d4-serotonin, and d4-melatonin, and 1,350 ng/mL for d5-HIAA in water by diluting 9 mL of the ISS-A

solution with 1 mL of water; this solution was used to prepare the combined intermediate solution and the Calibrators.

Stock solutions for acetyl-serotonin, 5-HIAA, 5-hydroxytryptophan, melatonin, serotonin, and tryptophan were each prepared at 10.0 mg/mL in water. A combined intermediate was prepared from each of the stocks at a concentrations of 100 μg/mL for each using Tryptophan Pathway ISS-B as the diluent. Calibrators were prepared from the combined intermediate by serial dilution (DF 4-fold per Calibrator level) at metabolite concentrations of 1,000, 250, 62.5, 15.6, 3.90, and 0.977 ng/mL using Tryptophan Pathway ISS-B as the diluent.

Stool sample extracts were thawed on the benchtop at ambient room temperature, and were vortex-mixed briefly. A 10-μL volume of stool sample extract was diluted in a 90-μL volume of the Tryptophan Pathway ISS-A solution directly in an autosampler vial, and the 10-fold diluted sample was vortex-mixed for 30 s. The samples were transferred to an autosampler and a 5-μL sample volume was injected onto the LC-MS/MS system for analysis.

The ion pairing-based reverse-phase separation for the measurement of Tryptophan Pathway metabolites was performed using an MPA solution consisting of water:ACN:FA:HFBA (99.3:0.5:0.1:0.1, *v:v:v:v*), a MPB solvent consisting of 100% ACN, and a NW consisting of ACN:water (1:1, *v:v*). Chromatographic separations were performed using a Luna C18(2) (150 mm × 1 mm, 3 μm) analytical column equipped with a C18 SecurityGuard™ (4 × 2 mm) guard cartridge. The mobile phase flowrate was 0.100 mL/min, the autosampler trays were chilled to 10°C, the column oven was heated at 50°C, and the gradient elution program used was 0-9.0 min, 5–60% MPB; 9.0–9.1 min, 60-5% MPB; 9.1–12.0 min, 5% MPB with a gradient cycle time of 12.4 min per sample. An ESI probe was installed and the 6500 QTrap MS was operated in positive ionization mode using an SRM scan mode with the following instrumental conditions: IonSpray voltage of +5,000 V; Cur: 20 psi; Temp: 200°C; GS1/GS2: 25 psi each; CAD gas: HIGH; and, Q1/Q3 resolution: Unit/Unit. See Table 4 for the metabolite specific SRM transition parameters for the Tryptophan Pathway metabolites.

LC-MS/MS method for the quantitation of tyrosine pathway metabolites

IS stock solutions for d4-dopamine, d6-epinephrine, d3-levodopa (L-DOPA), and d4-tyramine were each prepared at 10.0 mg/mL in water. An ISS-A solution was prepared from each of the IS stocks at a concentration of 125 ng/mL for d4-dopamine, 200 ng/mL for d6-epinephrine, 1,000 ng/mL for d3-L-DOPA, and 250 ng/mL d4-tyramine in water; the ISS-A solution was used in the final preparation of the microbiome samples. An ISS-B solution was prepared at a concentration of 112.5 ng/mL for d4-dopamine, 180 ng/mL for d6-epinephrine, 900 ng/mL for d3-L-DOPA, and 225 ng/mL d4-tyramine by diluting 9 mL of the ISS-A solution with 1 mL of water; this solution was used to prepare the combined intermediate solution and the Calibrators.

Stock solutions for anthranilic acid, dopamine, epinephrine, L-DOPA, norepinephrine, tyramine, and tyrosine were each prepared at 10.0 mg/mL in water. A combined intermediate was prepared from each of the stocks at a concentrations of 100 μg/mL for each using Tyrosine Pathway ISS-B as the diluent. Calibrators were prepared from the combined intermediate by serial dilution (DF 4-fold per Calibrator level) at metabolite concentrations of 1,000, 250, 62.5, 15.6, 3.90, and 0.977 ng/mL using Tyrosine Pathway ISS-B as the diluent.

Stool sample extracts were thawed on the benchtop at ambient room temperature, and were vortex-mixed briefly. A 10-μL volume of stool sample extract was diluted in a 90-μL volume of the Tyrosine Pathway ISS-A solution directly in an autosampler vial, and the 10-fold diluted sample was vortex-mixed for 30 s. The samples were transferred to an autosampler and a 5-μL sample volume was injected onto the LC-MS/MS system for analysis.

The ion pairing-based reverse-phase separation for the measurement of Tyrosine Pathway metabolites was performed using an MPA solution consisting of water:ACN:FA:HFBA (99.3:0.5:0.1:0.1, *v:v:v:v*), an MPB solvent consisting of 100% ACN, and a NW consisting of ACN:water (1:1, *v:v*). Chromatographic separations were performed using a Raptor C18 (100 mm × 1 mm, 2.7 μm) analytical column equipped with an Ultra C18 (10 mm × 2.1 mm, 5 μm) guard cartridge. The mobile phase flowrate was 0.200 mL/min, the autosampler

trays were chilled to 10°C, the column oven was heated at 40°C, and the gradient elution program used was 0-0.5 min, 5% MPB; 0.5–6.0 min, 5–90% MPB; 6.0–7.0 min, 90% MPB; 7.0–7.1 min, 90-5% MPB; 7.1–12.0 min, 5% MPB with a gradient cycle time of 12.4 min per sample. An ESI probe was installed and the 6500 QTrap MS was operated in positive ionization mode using an SRM scan mode with the following instrumental conditions: IonSpray voltage of +5,000 V; Cur: 20 psi; Temp: 300°C; GS1/GS2: 25 psi each; CAD gas: HIGH; and, Q1/Q3 resolution: Unit/Unit. See Table 5 for the metabolite specific SRM transition parameters for the Tyrosine Pathway metabolites.

Metabolite networks

Neurotransmitter and SCFA concentrations were first decile scaled across fecal samples collected from mice in each group (n = 3 SPF mice, n = 5 germ-free mice, n = 5 *B ovatus* mono-associated mice). These deciles were then imported into the program Cytoscape (Shannon et al., 2003) (version 3.8.2) as edge weights in order to generate a mouse microbiome-metabolites bipartite network. The layout was generated with the Edge-weighted Spring Embedded Layout algorithm.

QUANTIFICATION AND STATISTICAL ANALYSIS

Statistical analysis and graphical representation of experimental data were performed with GraphPad Software (GraphPad Software, Inc. La Jolla, CA). Data are presented as mean ± stdev, n = 3 replicates for *in vitro* bacterial culture experiments and n = 5 mice/group for *in vivo* studies. *$p < 0.05$, **$p < 0.01$, ***$p < 0.001$, ****$p < 0.0001$. Comparisons between groups were made using One-way or Two-way Analysis of Variance (ANOVA), using the Holm-Sidak *post-hoc* test comparisons.